Journal of Physics D: Applied Physics

Genetically encoded single circularly permuted fluorescent protein-based intensity indicators

To cite this article before publication: Wenfeng Liu *et al* 2019 *J. Phys. D: Appl. Phys.* in press https://doi.org/10.1088/1361-6463/ab5dd8

Genetically encoded single circularly permuted fluorescent protein-based intensity indicators

Wenfeng Liu[1,#], Mengying Deng[1,#], Chengming Yang[2,#], Feng Liu[1], Xinmeng Guan[1], Yichen Du[3], Liang Wang[1,*], Jun Chu[1,4,*]

[1] Laboratory for Biomedical Optics and Molecular Imaging, Shenzhen Institutes of Advanced Technology, Chinese Academy of Sciences, Shenzhen, 518055, China
[2] Department of Ophthalmology, Southern University of Science and Technology Hospital, Shenzhen, 518055, China
[3] Department of Biology, Southern University of Science and Technology, Shenzhen, 518055, China
[4] CAS Key Laboratory of Health Informatics, Shenzhen Institute of Synthetic Biology, Shenzhen-Hong Kong Institute of Brain Science, Shenzhen Institutes of Advanced Technology, Chinese Academy of Sciences, Shenzhen, 518055, China
[#] These authors contributed equally to this work.
[*] Correspondence: liang.wang1@siat.ac.cn or jun.chu@siat.ac.cn.

Abstract

Fluorescent protein (FP)-based genetically encoded indicators are valuable tools for reporting signaling activities with high spatial-temporal resolution in living cells and animal models. Thereinto, single circularly permuted FP-based intensity sensors (cpFP sensors or cpFP-based sensors, unless otherwise specified) are of particular interest due to their unprecedented high sensitivity and fast kinetics. In this review, we summarized the recent progress with cpFP sensors, focusing on the practical considerations in sensor development and usage, and categorization of cpFP sensors. We also discuss future directions in improvement of existing sensors, development of new sensors, and functional super-resolution imaging with cpFP sensors.

Key words

fluorescent protein, circular permutation, cpFP, genetically encoded indicator, GCaMP

1. Introduction

The concentration and activities of signaling molecules such as second messengers and kinases, which are tightly regulated in space and time, are essential for cell function. Real-time non-invasive visualization of signaling molecules in living cells and tissues advances our understanding of the molecular mechanisms underlying normal physiology and diseases. Thanks to the development of fluorescent proteins (FPs) and advanced microscopy, various FP-based indicators, which are genetically encoded, have been developed to monitor signaling activities not only in living cells but also in small animals with high spatiotemporal resolution[1-4]. Compared to non-protein-based sensors, genetically encoded ones have several advantages. First, they can be relatively easily constructed via genetic engineering, introduced into cells or tissues by standard transfection techniques or by virus-mediated gene transfer, and integrated into the cell

genome. Second, they have relatively low cytotoxicity and low background fluorescence due to their lack of need for exogenous co-factors[5]. Third, they exhibit high cellular and subcellular specificity via cell-specific promoters and subcellular targeting sequences, respectively, which enables exploration of activity patterns in cells of interest in tissues and regions of interest in cells.

Certain FPs themselves are intrinsically sensitive to specific molecules or environments to some extent and can be engineered to highly sensitive indicators, such as the pH sensor pHluorin[6]. FPs can also be devised to act as sensors for certain analytes via introducing specific unnatural amino acids, such as the H_2S probe hsGFP[7,8]. However, these methods are not broadly applicable. To overcome this limitation, several strategies, which involve fluorescence modulation through conformation or distance change of FP moieties mediated by an analyte- or activity-sensing module, have been developed[5]. Of these, Föster resonance energy transfer (FRET)[9], bimolecular fluorescence complementation (BiFC)[10], dimerization-dependent fluorescence increase (DDFI)[9,11] and fluorescence fluctuation increase by contact (FLINC)[12], require proximity between two FPs (FRET/DDFI/FLINC) or two non-fluorescent fragments of a FP (BiFC) and thus are highly distance-dependent (Fig. 1). However, the fluorescence signal change of these techniques is either irreversible (BiFC) or usually small in mammalian cells[9,13]. Moreover, the kinetics of some indicators is often slow due to the physical movement of two FPs or FP fragments that is required[3].

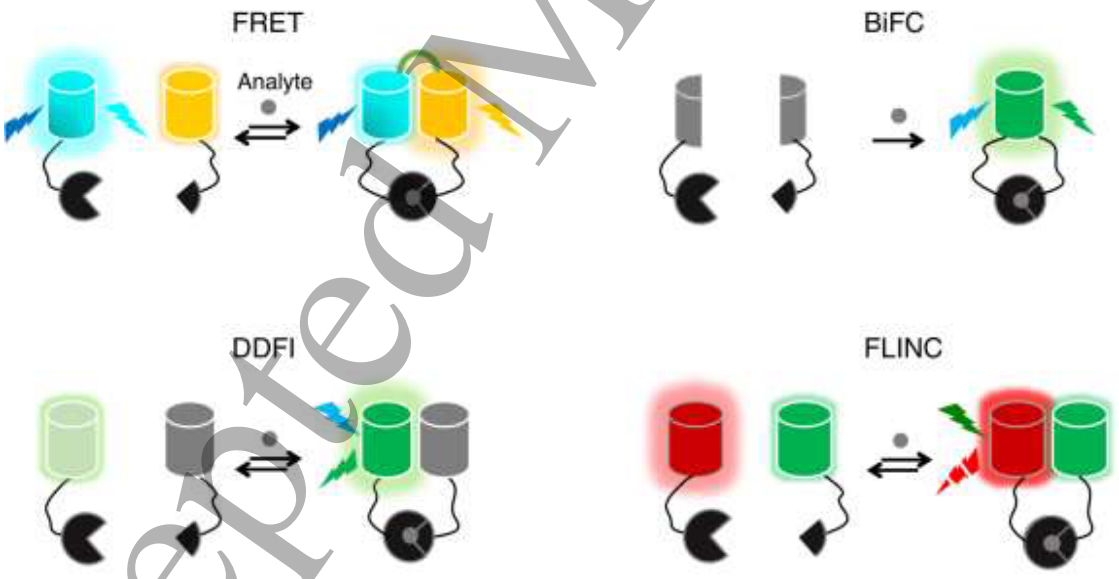

Figure 1 Four different FP-based assays that are distance-dependent. The interaction in the sensing module (black) brings two FPs (or two FP fragments in BiFC) into proximity upon analyte binding, generating FRET, BiFC, DDFI and FLINC. The excitation light and emitted fluorescence are indicated by lightning bolts. In FLINC, the blinking fluorescence is indicated by a broken lightning bolt.

An alternative strategy is to take advantage of circularly permuted FP (cpFP), which is generated by linking the original N- and C- termini with a flexible linker and introducing new N- and C- termini either at the midpoint of β strand 7 (e.g., GFP and GFP-like FPs, Fig. 2A,B) or in surface-exposed loop regions (e.g., near-infrared FP mIFP, Fig. 2B). A

typical cpFP-based indicator consists of a sensing module and a single cpFP, which are attached to each other by two peptide linkers (Fig. 2C). In cpFP sensors, analyte- or activity-induced conformational or distance change of the sensing module is transduced to cpFP through linkers and changes the environment around the chromophore, leading to either a shift in the protonation/deprotonation equilibrium of the chromophore, a change in extinction coefficient (EC), or a change in quantum yield (QY)[14].

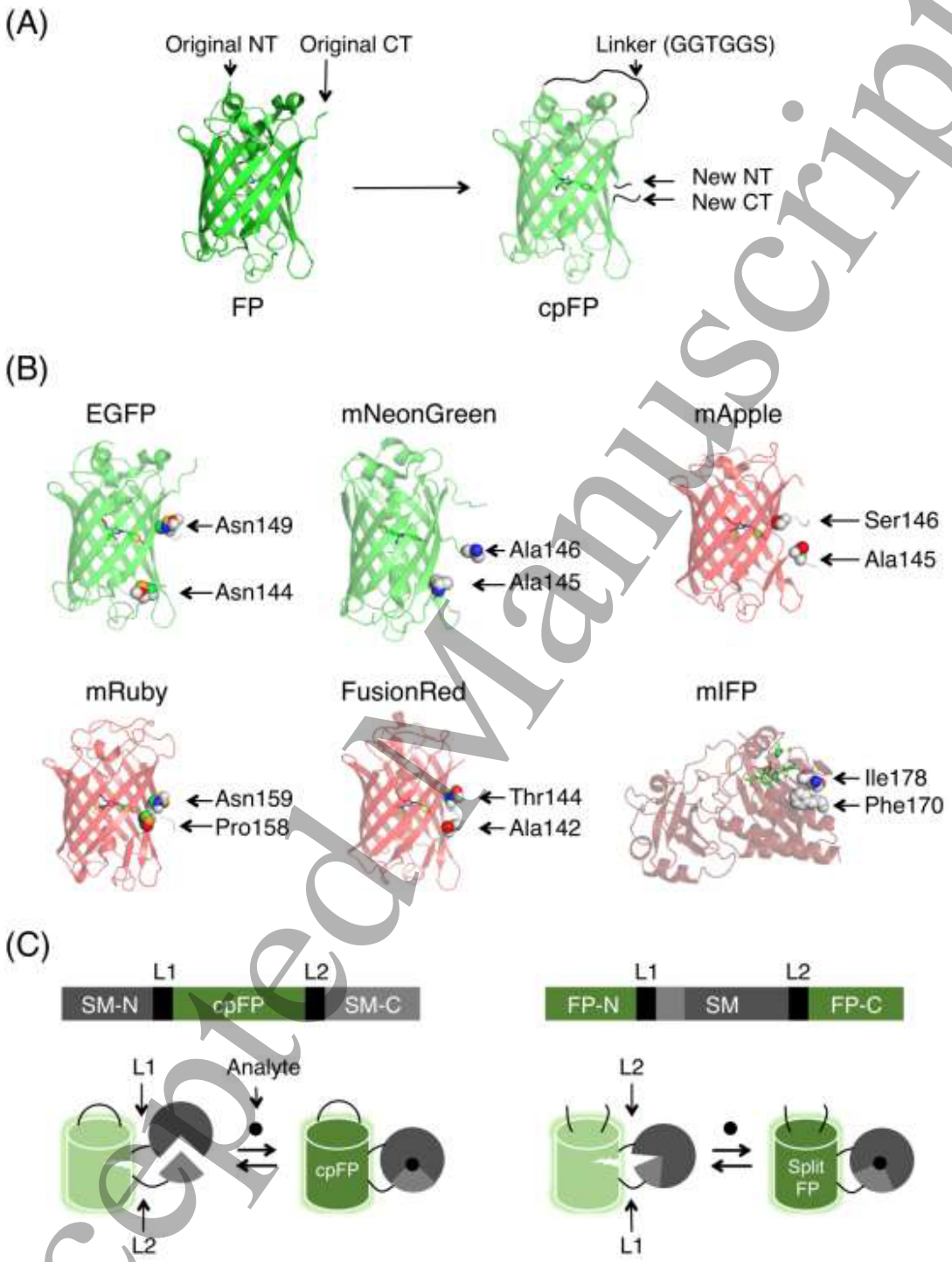

Figure 2 Schematic structures of cpFP, circular permutation sites of FPs and cpFP sensors. (A) The original N- and C- termini are linked through a flexible linker GGTGGS, and the new N- and C-termini are introduced at the midpoint of β strand 7. The chromophore is shown as stick. The structure is based on PDB entry 2Y0G. (B) Circular permutation sites of green, red and near-infrared (NIR) FPs**.** EGFP (PDB: 3WLD) and mNeonGreen (PDB: 5MWC) are two green FPs derived from *Aequorea victoria* GFP (avGFP) and *Branchiostoma lanceolatum* YFP (LanYFP), respectively. mApple (PDB: 4I2Y), mRuby (PDB: 3U0K) and FusionRed (PDB: 5UKG) are representative ones of three major lineages of red FPs derived from

Discosoma sp. RFP (DsRed), *Entacmaea quadricolor* RFP (eqFP611) and *Entacmaea quadricolor* RFP (eqFP578), respectively. mIFP (structure modeled based on PDB entry 2O9B) is a NIR FP derived from *Bradyrhizobium* bacteriophytochrome (*Br*BphP). Chromophores and circular permutation sites are shown as stick and sphere, respectively. Note: the nonadjacent breakpoint for cpEGFP shown here is true only for calcium sensors (GCaMPs) and cGMP sensors (FlincGs). All other cpEGFP-based sensors have a complete β-barrel, such as in voltage sensors (ASAPs). The function of His148 in cpEGFP of GCaMPs is replaced by an Arg from CaM and a water molecule, which is unusual. (C) cpFP sensors can be constructed either by inserting a cpFP into a sensing module (SM) (left) or a SM into a FP (right). NT, N-terminus. CT, C-terminus. SD-N and SD-C are the N-terminal and C-terminal fragment of a SM, respectively. FP-N and FP-C are the N-terminal and C-terminal fragment of a FP, respectively. L1 and L2 are the linkers between SM and cpFP.

cpFP sensors feature large signal change, fast kinetics and a single color, providing a powerful way to visualize single signaling molecules and monitor multiple events with spectrally distinct probes. Although cpFP indicators have been an important and fast-growing area of research, no extensive reviews on cpFP indicators have been reported thus far. In this review, we first briefly describe the sensor design strategies and screening methods for cpFP indicator development, systematically discuss key biochemical and photophysical properties of cpFP sensors, then summarize current cpFP sensors for various analytes and molecular activities, and finally envision future directions for this rapidly growing area.

2. cpFP indicator development

Like other genetically encoded sensors, an ideal cpFP indicator should have good folding and maturation, good trafficking, low cytotoxicity, high signal-to-noise ratio, great photostability, high sensitivity (large dynamic range and appropriate affinity), fast kinetics, and high specificity. Each property is to some extent attributed to different components of the cpFP indicator, including the sensing module, cpFP, the linkers and interface between them, and even the purification tag (e.g. the RSET leader sequence in calcium sensor GCaMP). Hence, to obtain ideal high-performance cpFP sensors, all components should be carefully chosen and/or optimized.

2.1 Design and optimization strategies

Based on the position of the sensing module relative to FP in protein sequence, cpFP indicators can be classified into two categories (Fig. 2C). One is the insertion of a cpFP into the appropriate site of a sensing module (Fig. 2C, left), such as the state-of-the-art calcium sensor GCaMPs[15,16]. The other one is the insertion of a sensing module into a FP (Fig. 2C, right), in which the sensing module is flanked by two split FP fragments. This strategy was prominently illustrated in the sensors developed by Tetsuya Kitaguchi group, such as Flamindos for cAMP, cGulls for cGMP, MaLions for ATP, and Glifons for glucose, and by Robert Campbell group, such as GINKO1 for potassium ion (K^+) and NIR-GECO1 for calcium ion (Ca^{2+}) [17-23]. In practice, although both designs have similar overall protein structures, the former design is preferred and more common because cpFP itself has better folding than split FP and does not require the two termini of sensing module to be close to one another[10]. However, compared to split FP-based

indicators, CP ones may have two disadvantages[23]. In a CP topology, only the sensing module has free termini and thus may be more likely to interact with endogenous protein binding partners and lead to perturbations of normal protein functions ([23,24], and also may adversely affect the performance of the indicator itself when fused to organelle targeting sequences or proteins of interest.

Green (or yellow) FPs and red FPs have been most commonly used as cpFPs because their well-separated spectra allow for dual-color imaging (Table 1). Each class has distinct advantages and disadvantages. Green/yellow sensors usually show better cellular localization in mammalian cells, higher cellular brightness and larger dynamic range, while red ones exhibit lower background and are spectrally compatible with blue/green light-activatable optogenetic tools, enabling simultaneous optical stimulation and recording[25,26]. Near-infrared (NIR) cpFP sensors are also of great interest because their peak fluorescence falls within the NIR-I window (650 nm - 900 nm), which is suitable for deep-tissue imaging (Table 1)[23]. More importantly, one-photon epifluorescence imaging with NIR cpFP sensors has much higher temporal resolution than two-photon imaging with green/red ones, enabling large-field-of-view NIR imaging of fast biological events *in vivo*.

Table 1 Fluorescent proteins used for cpFP indicators mentioned in this review

FP	Ex (nm)	Em (nm)	EC ($mM^{-1}cm^{-1}$)	QY	Molecular Brightness	pKa	Ref.	Comment
BFP	381	445	14	0.38	5.32	4.9	[27]	Derived from EGFP
T-Sapphire	399	511	44	0.60	26.40	4.9	[28]	Derived from EGFP
mEGFP	488	507	55.9	0.60	33.54	6.0	[29]	Mostly used FP
sfGFP	488	510	83.3	0.65	54.15	5.9	[30]	Derived from EGFP. Better folding
mNeonGreen	506	517	116	0.80	92.80	5.7	[31]	Brightest green FP
EYFP	513	527	67	0.67	44.89	6.9	[32]	Derived from EGFP. Not photostable
Citrine	516	529	77	0.76	58.52	5.7	[33]	Derived from EGFP. Not photostable
Venus	515	528	92.2	0.57	52.55	6.0	[34]	Derived from EGFP. Not photostable
mApple	568	592	75	0.49	36.75	6.5	[35]	Photoswitchable, aggregation
mRuby	558	605	112	0.35	39.20	4.4	[36]	
FusionRed	580	608	94.5	0.19	17.95	4.6	[37]	Best RFP for cpFP
mEos2 (green)	506	519	56	0.84	47.04	5.6	[38]	Photoconvertible
mEos2 (red)	573	584	46	0.66	30.36	6.4		
mIFP	683	704	82	0.08	6.56	3.5	[39]	Bacteriophytochrome-based; low brightness

FP, fluorescent protein. Ex, excitation peak. Em, emission peak. EC, extinction coefficient. QY, quantum yield. Molecular brightness, a product of EC and QY. pKa, pH at which the fluorescent intensity is 50% of its maximum value.

The sensing module could be the analyte or activity-sensing domain from a single protein or a sensing domain (or peptide) with its interaction partner from two proteins (Fig. 3). For cpFP sensors, non-mammalian sensing modules are preferred because they are assumed to be unlikely to interfere with signaling pathways in the mammalian cells used in most studies. A big challenge for the sensing modules is that modules may exhibit different biochemical properties including affinity and/or become insoluble or poorly folded when isolated from their native proteins. Therefore, the sensing module should be

carefully chosen, with good solubility or folding, high selectivity, appropriate affinity or sensitivity and fast kinetics toward the analyte or molecular activity. Moreover, it should express well with correct cellular localization and low cytotoxicity in cells of interest when fused to cpFP.

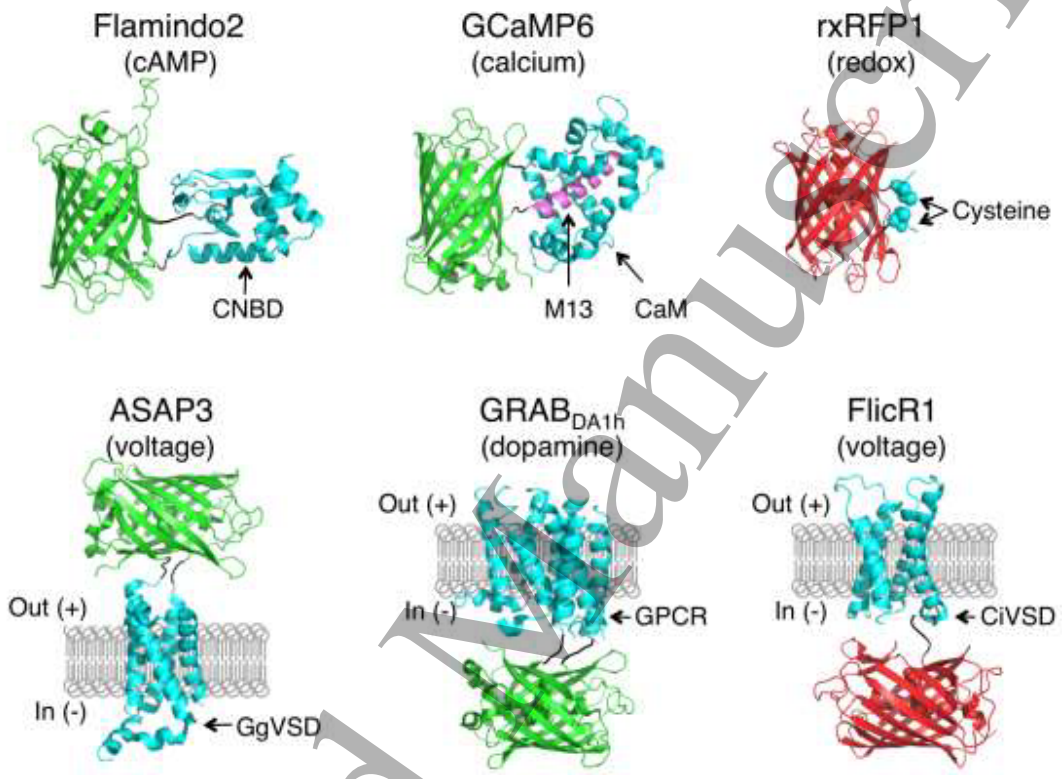

Figure 3 Representative cpFP indicators with different sensing modules. The sensing modules in cpFP indicators differ in their sensing mechanism (conformational change of a single domain or interaction between two domains or peptides, Flamindo2 vs GCaMP6), subcellular localization (plasma membrane or non-plasma membrane, rxRFP1 vs ASAP3), or fusion pattern (both ends of cpFP fused with the sensing module or only one end of cpFP fused with the sensing module, $GRAB_{DA1h}$ vs FlicR1). Sensing modules are marked in cyan, cpFPs are colored in green or red, and the linkers between cpFP and sensing module are marked in black. CNBD, cyclic nucleotide binding domain. GgVSD, *Gallus gallus* voltage-sensing domain (VSD). CiVSD, *Ciona intestinalis* VSD. GPCR, G protein-coupled receptor. Analytes or molecule activities detected are shown in the brackets.

The insertion (or fusion) site in sensing module and linkers between the sensing module and cpFP are essential for the conformation transduction process and thus are directly linked to the performance of a given sensor. Generally speaking, a cpFP sensor could start with a flexible linker such as GS or a known linker from existing cpFP sensors while the insertion site is sensing module-dependent. For the sensing module with single domain, although tandem fusion of cpFP and sensing module works for some indicators, it is more common to insert the cpFP into loop regions near the binding pocket that undergoes substantial conformational changes to generate large dynamic ranges (Fig. 3, ASAP3 and $GRAB_{DA1h}$). For the sensing module with two domains (or peptides), just

attach two parts of sensing module to two ends of cpFP with appropriate linkers (Fig. 3, GCaMP6).

Once the protein fusion is done, site-directed and random mutagenesis on the sensing module, the cpFP, the linkers and interface between them are necessary to improve the indicator's performance. However, these components are potentially the most challenging parts to optimize because they are tightly associated with each other and their effects may conflict with each other. In practice, this could be performed step by step, depending on the goals. One of the most desired properties is a large dynamic range, which is closely related to the linkers between cpFP and sensing module. Extensive screening of the linkers could lead to indicators with very large dynamic range, decent brightness, and good kinetics[13]. To further improve the brightness and/or dynamic range, structure-guided mutagenesis of the fluorescent protein can be performed. To tune the affinity and kinetics of the sensor, site-directed mutations of the binding pocket or activity-modulating motif in the sensing module could be helpful. In this way, one could even change the specificity of a sensor while retaining other properties such as dynamic range[40]. Lastly, the interface between the sensing domain and cpFP requires engineering to be optimal. If crystal structures of an indicator are available, rational computational design of the interface can also improve some key sensor properties, such as basal and peak intensities and kinetics[16].

2.2 Screening strategies

Unlike FRET indicators, the evolution of cpFP indicators requires large-scale mutational screening, which is labor-intensive and time-consuming (Fig. 4)[13]. Thus, high-throughput screening techniques for library construction, sensor characterization, and cell picking are highly desired.

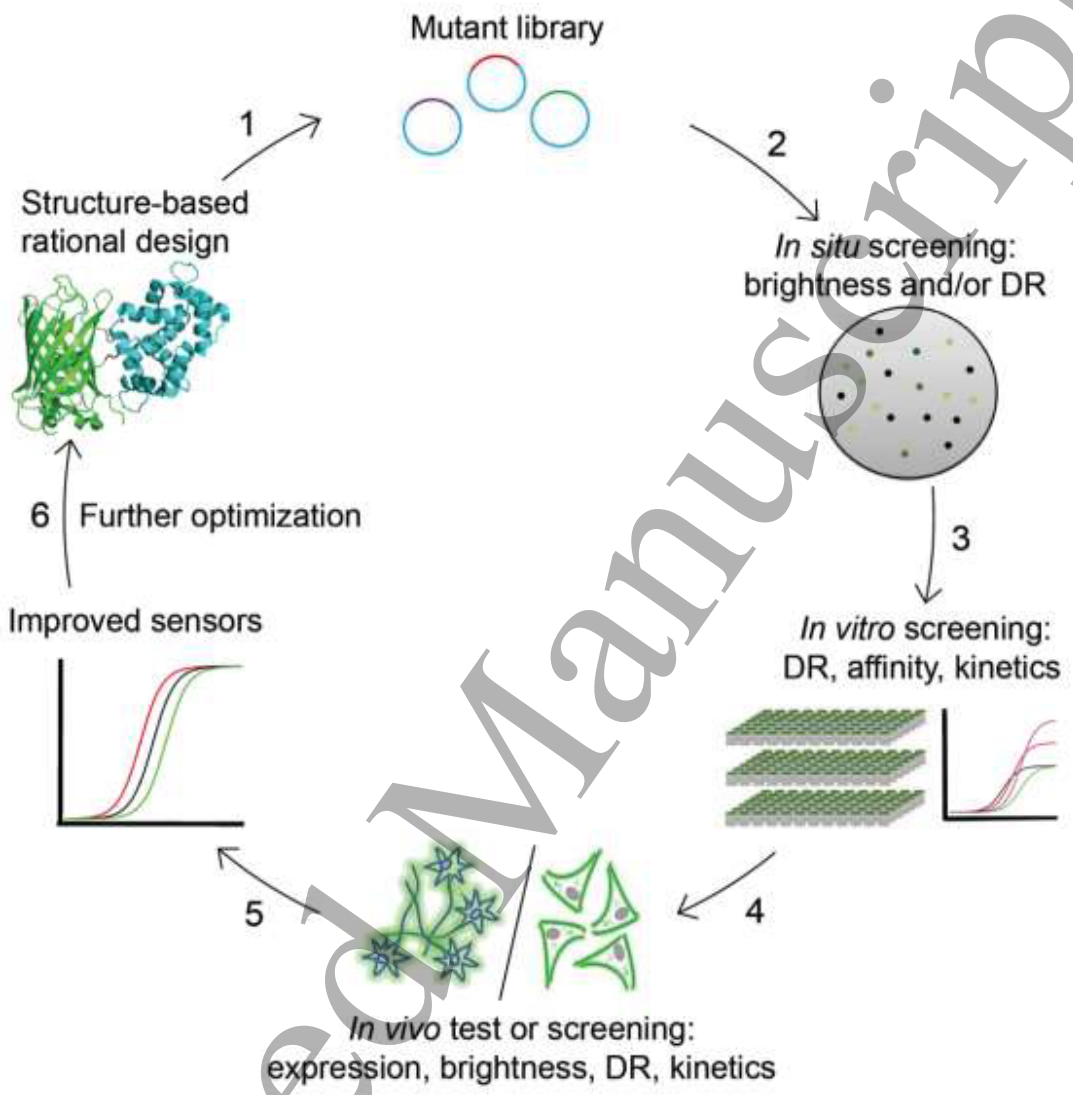

Figure 4 General workflow of the cpFP sensor evolution. Different properties could be tested in bacteria, *in vitro*, or in mammalian cells.

The bacterium *Escherichia coli* (*E. coli* for short) grows fast and has high transform efficiency, being the first choice for engineering FP-based sensors[26]. Fluorescent colonies expressing cpFP sensors can be picked on the plate either manually or by imaging-guided automatic robotic picking device, or sorted in solution by flow cytometry[41-43]. Photostability can also be improved in bacteria either on plate or in solution[44,45]. However, single colony-based *in-situ* optimization of dynamic range is very challenging due to the difficulty of simultaneously and rapidly manipulating the analyte concentrations of all colonies on the plate. One easy and effective way is to direct cpFP sensor into the bacterial periplasm and then spray plates with small analytes or other molecules which can readily cross bacterial cell wall into the periplasm and change the analyte concentration. This idea was first introduced and demonstrated in calcium

sensors[26]. However, this approach is not suitable for cpFP indicators with poor folding in the periplasm or molecules with low crossing efficiency. An alternative way is a multi-well plate-based assay with four steps: fluorescent colonies are picked, grown directly in multi-well plates, lysed in situ and mixed with analyte. For indicators used in mammalian systems, desirable variants screened from bacteria should be further tested in mammalian cells due to substantial environment differences between these two cell types. To minimize the cloning steps, a DNA vector that is capable of expressing sensors in both *E. coli* and mammalian cells has been developed[23].

Some cpFP sensors do not express well in *E. coli* and yeast, such as G protein-coupled receptor (GPCR)-based neurotransmitter sensors (personal communication with Yulong Li at Peking University), or *E. coli* does not possess certain specific activities, such as action potential (AP) in neurons. In these cases, sensor variants should be screened in mammalian cells, such as easy-to-transfect HEK293 cells or neurons. For example, HEK293 cells were used to optimize the plasma membrane localization, dynamic range and brightness of GPCR-based sensors and neurons were for ultrasensitive GCaMPs[16,46]. However, these methods are usually limited in throughput because mutants must frequently be tested manually one-by-one in cells, especially for neurons that are experimentally intractable. To overcome these limitations, in 2018, two groups independently developed HEK293 cell-based automatic robotic systems, integrating electrical stimulation, imaging, data analysis and cell picking to improve the performance of voltage sensors[47,48]. Interestingly, instead of plasmids, PCR products without purification can be directly used for cell transfection and greatly speed up library construction[48]. Although both robotic systems are optimized for voltage sensors, in principle, they could be applied to non-voltage sensors with minimal adaption.

3. Considerations when using cpFP indicators

Like other genetically encoded sensors, cpFP ones have their own strengths and weakness. Moreover, for the same analyte or molecule activity, several cpFP sensors could be available. Therefore, cpFP sensors should be carefully considered and chosen based on their properties and research purpose.

3.1 Intensiometric and ratiometric readout

Many cpFP sensors are intensiometric as they rely on the readout of single fluorescence emission by single wavelength excitation. However, the intensiometric readout may result in data misinterpretation in long-term imaging as the fluorescence change could be due to motion or morphology change[49]. This issue is commonly addressed by converting sensors from intensiometric to ratiometric. A simple way is to fuse cpFP sensors with a spectrally well-separated FP, such as mCherry in the case of green sensors. However, the reference FP and its attached linker should be carefully chosen to minimize FRET[50]. To overcome this problem, a rigid linker attached to a regular reference FP and a blue-excitable orange/red FP as a reference have been utilized. Jung-Hwa Cho *et al* (2017) fused GCaMPs to mCherry with a rigid α-helix to eliminate FRET[50]. Cindy Ast *et al* (2017) inserted a blue-excitable orange FP LSSmOrange into the flexible linker

(GGTGGS) of cpFP in the CCaMPs without significantly affecting the affinities and dynamic ranges and demonstrated the ratiometric imaging with single wavelength excitation, retaining good temporal resolution by avoiding the sequential imaging of GCaMP and mCherry[51].

3.2 Upward and downward indicators

The fluorescence of cpFP sensors can increase (upward) or decrease (downward) as the analyte concentration or molecular activity increases. The downward one with high resting fluorescence is preferred when precise localization of cells *in vivo* or subcellular structures is needed. However, this kind of sensors is prone to photobleaching because of their stronger absorption compared to upward ones' in the resting state. Moreover, they have low signal change due to unexpected fluorescence signal from neighboring cells. On the contrary, the upward one overcomes the above limitations. Moreover, its low brightness in the resting state can be easily addressed by co-expressing a bright reference FP.

3.3 Signal-to-noise ratio

Three key factors including fluorescence signal (F), noise (N) and background fluorescence (B) influence the quality of fluorescence images, where the intensity value of each pixel is equal to the signal plus the background. Unlike signal, which has a single source, the background can come from many sources such as autofluorescence and out-of-focus fluorescence. Fluorescence intensity varies in repeated measurements of an unchanging specimen. This variation, referred to as noise, imposes an uncertainty in the quantification of fluorescence signal. The noise has three major components: dark noise, read noise and shot noise. Most scientific cameras have very little dark and read noise, leaving shot noise as the key source. Shot noise cannot be reduced or removed and is proportional to the square root of the number of photons hitting the camera, regardless of whether they are signal photons or background photons[52].

To detect the presence of a signal, the signal must be significantly higher than the noise level of the digital image, which is quantified by signal-to-noise ratio (SNR)[52]. In the case of cpFP sensor, SNR is given as the ratio of the change in fluorescence upon stimulation over the (or estimated) shot noise, and can be expressed in three different ways: $SNR=\Delta F/(F_0+B)^{1/2}$[53], or $SNR=\Delta F/$(standard deviation of $(F_{01}\ldots F_{0n})$)[54], or $SNR=\Delta F/(F_0/N^{1/2})$[55,56], where ΔF is the fluorescence change (F_1-F_0) between peak fluorescence (F_1) upon stimulation and average (F_0) of a set of baseline fluorescence signals ($F_{01}\ldots F_{0n}$), B is the background fluorescence, and N is the number of photons collected.

3.4 Sensitivity

Sensitivity is mainly determined by dynamic range and the midpoint of the response curve (F-Analyte concentration or F-Molecule activity), and usually characterized by the signal change ($\Delta F/F_0$) in living cells. Dynamic range refers to the fluorescence intensity

change between the fully saturated and unbound states of a sensor *in vitro* and can be measured by the ratio of the fluorescence signals in these two states. The midpoint of the response curve is typically measured and reported by the equilibrium dissociation constant (K_d) or concentration for 50% of maximal effect (EC_{50}) in the case of analyte. To ensure high sensitivity, besides large dynamic range, the midpoint of the response curve of a selected cpFP sensor is better to be either around the physiology concentration of the analyte or near the resting molecule activity in cells[16,57]. For example, ultrasensitive GCaMP6s (K_d = 144 nM) or jGCaMP7s (K_d = 68 nM) are useful to report calcium changes in the cytoplasm (~ 50-100 nM at rest)[58], but not good for those in ER (~ 60-400 μM)[59].

cpFP sensors with good folding and trafficking also increase the sensitivity by reducing unresponsive fluorescent probes in cells, which is especially true for localization-specific sensors. For example, better trafficking of voltage sensor to plasma membrane increased voltage sensitivity[53].

3.5 Kinetics

Association and dissociation rate constant (k_{on} and k_{off}) or signal rise and decay time (τ_{on} and τ_{off}) are commonly used to measure the response kinetics of the indicator toward analytes or activities. To report the dynamics of analyte or molecular activity accurately, the indicator should have a sufficiently fast kinetics. For example, it's important for voltage sensors to have τ_{on} and τ_{off} with millisecond or sub-millisecond response because of the ultrafast action potential firing. Otherwise, it is difficult to resolve the successive voltage spikes under high-frequency pulse-train stimulation[53].

The kinetics is related to the dissociation constant K_d, which is given as the ratio of k_{off} and k_{on}[60]. For example, the dopamine (DA) indicator $GRAB_{DA1h}$ has a higher affinity than $GRAB_{DA1m}$ (10 nM vs 130 nM), but has a slower ON kinetics (140 ms vs 60 ms)[46]. Therefore, from a practical view of point, it is challenging for a single cpFP sensor to achieve both fast kinetics and high affinity.

3.6 Linearity

In general, linearity is described as Hill coefficient (n_H), which measures the degree of cooperativity in a binding process and can be derived from the dose-response curve[61]. Indicators with an n_H around 1 would give a linear response for a wider stimulus range than ones with an n_H much larger than, allowing the direct determination of absolute changes in analyte from the relative changes in fluorescence. For example, the calcium sensor XCaMP-Gf (n_H ~1.4) showed a more linear response than GCaMP6f (n_H ~3.1) in response to high-frequency stimulation in neurons[62].

3.7 Specificity

A highly specific or selective cpFP indicator, which has much higher affinity for analyte of interest over other molecules, is highly desired. However, in some cases, an indicator

with similar affinities toward different analytes can still work as long as unwanted analytes in cells have extremely low concentration and are maintained at low levels upon stimulation compared to the desired one[46].

3.8 Photostability and Brightness

Intense illumination causes irreversible loss of fluorescence signal, a process called photobleaching, which could complicate the data analysis. To alleviate this problem, photostable and/or bright sensors are highly required (e.g. bright calcium sensor jGCaMP7b), especially in fast time-lapse imaging of small size subcellular structures such as the synapse, where intense illumination or long exposure time is required to obtain high fluorescence signal. However, cpFP sensors with dim basal fluorescence signal would be particularly useful (e.g., dim jGCaMP7c) in the case of densely labeled samples as large signal change ($\Delta F/F_0$) can be achieved due to low background fluorescence from out-of-focus planes and neighboring cells under epifluorescence imaging[63].

Besides photobleaching, light can also induce phototransformations such as photoactivation or photoswitching, which causes artificial photobleaching and should be avoided during the recording period if quantitative analysis is needed. Therefore, photoswitchable red FP mApple-based cpFP sensors should be carefully considered before usage.

3.9 pH stability

One weakness of many cpFP sensors is their low pH stability, usually with a pKa ranging from 6 to 10 because cpFP is not intact as its none-CP version and is thus more environment-sensitive. This should be carefully considered when a stimulus induces intracellular pH change. In most cases, this effect is ignored. If necessary, this pH vibration-induced intensity changes can be corrected by taking account of the fluorescence intensity change from a control sensor without binding ability or a corresponding cpFP with similar pH sensitivity[40,64].

4. Current cpFP indicators

4.1 Ca^{2+} indicators

Calcium is an important second messenger that regulates many cell functions, including fertilization, proliferation, communication and apoptosis. Cytosol calcium either is released from intracellular stores, or enters the cell via plasma membrane ion channels. The first cpFP-based genetically encoded calcium indicator (GECI) came from Geoffrey S. Baird *et al* (1999), in which the authors inserted *Xenopus* calmodulin (CaM) into enhanced yellow fluorescent protein (EYFP)[65]. Indeed, this was the first cpFP sensor. Inspired by this, Takeharu Nagai *et al* (2001) and Junichi Nakai *et al* (2001) developed cpYFP- and cpEGFP-based Ca^{2+} indicators, respectively[15,66], in which the N- and C-termini of cpFP were connected to CaM and the M13 (derived from the skeletal muscle

myosin light chain kinase), respectively[67]. Further mutagenesis on the above cpEGFP-based indicator (also known as GCaMP1) led to GCaMP2 (2006) and GCaMP3 (2009) with higher brightness and/or larger dynamic ranges in mammalian cells (Table 2)[57,68]. Most of the beneficial mutations are in the cpEGFP domain and one in the CaM motif (N60D). More extensive structure-guided mutagenesis (mainly focusing on the cpGFP-CaM and CaM-M13 interfaces) and screening in dissociated neurons resulted in ultrasensitive and bright GCaMP6 series (2013) and jGCaMP7 series (2018) sensors (Table 2), which are capable of detecting Ca^{2+} signal induced by a single action potential[16,63]. Moreover, the recently developed green XCaMPGf GECI based on the G-CaMP4.1 backbone with the M13 replaced by ckkap peptide, which is derived from CaMKK-α with higher affinity for Ca^{2+}-bound CaM, has an n_H of 1.4 and showed improved linearity compared to GCaMP6f ($n_H \sim 2.27$)[62]. In all these new generations of GECIs, their properties such as brightness, dynamic range, affinity and rise/decay kinetics, are highly optimized for specific applications (Table 2).

Besides the green GECIs mentioned above, red and near-infrared ones were also developed. Red cpFP sensors are mainly based on three lineages of RFPs such as mRuby, mApple, and FusionRed and can be classified into three classes: I) RCaMPs including RCaMP1h (2013) and jRCaMP1a/b (2016), II) R-GECO1 (2011), R-CaMP1.07 (2012), jRGECO1a (2016) and R-CaMP2 (2015), XCaMP-R (2019), III) K-GECO1 (2018) (Table 2)[25,26,36,62,69-71]. Of these, class I has limited sensitivity and class II shows lysosomal accumulation and photoswitching. Class III K-GECO1 overcomes these drawbacks to a large extent while maintains comparable sensitivity and kinetics to other highly optimized red GECIs. In R-CaMP2, XCaMP-R and K-GECO1, the commonly used M13 was replaced by ckkap peptide. Remarkably, all the three sensors have an n_H near 1, suggesting the linear response in ckkap-derived GECIs. Very recently, Yong Qian *et al* (2019) developed the first NIR calcium indicator NIR-GECO1 by inserting the Ca^{2+}-binding module (CaM and RS20 derived from the smooth muscle myosin light chain kinase) into a bacteriophytochrome-based NIR fluorescent protein mIFP[23]. However, the overall performance of NIR-GECO1 is inferior to GCaMP6 and requires further improvements in brightness, photostability and kinetics.

In parallel to the development of calcium sensors with regular FPs, phototransformable FP-based sensors have also been explored. Shai Berlin *et al* (2015) developed a photoactivatable sPA-GCaMP6f sensor while retaining the Ca^{2+}-sensing ability[72]. With this sensor, neurons of interest *in vivo* can be easily selected from dense cell populations by UV light (~ 400 nm) and their activities can then be recorded with blue light illumination. Benjamin F. Fosque *et al* (2015) and Benjamien Moeyaert *et al* (2018) developed photoconvertible EosFP-based CaMPARI/CaMPARI2 sensors, which irreversibly changes its color from green to red upon UV light illumination only in calcium bound state[73,74]. Using this probe, active neurons in a large tissue volume within a given time window were successfully labeled as red by the UV light.

Despite the great success of cpFP GECIs, cpFP GECIs possess an intrinsic disadvantage that the apo form of CaM domain interferes with L-type calcium channels signaling in neurons, and thus leads to undesired side-effects such as cell damage and abnormal

neuron functions. By incorporating an extra apoCaM-binding motif, Yaxiong Yang *et al* (2018) constructed GCaMP-X sensors which eliminates apoCaM interference[24].

Table 2 Summary of representative cpFP-based calcium sensors.

Indicator	Analyte	Sensing module	cpFP	$\Delta F/F_0$ *in vitro/in vivo*	K_d *in vitro*	n_H	τ_{on}/τ_{off}	Year	Ref.
EYFP–calmodulin	Ca^{2+}	*Xenopus* calmodulin	Split EYFP	6/6	7 μM	1.6	ND/ND	1999	[65]
G-CaMP (GCaMP1)	Ca^{2+}	CaM/M13	cpEGFP	3.5/4	235 nM	3.3	<10 ms[a]/200 ms	2001	[15]
GCaMP3	Ca^{2+}	CaM/M13	cpEGFP	12.5/5.6(160 AP)	660 nM	2.54	137 ms/597 ms(10 AP)	2009	[57]
GCaMP6s (slow)	Ca^{2+}	CaM/M13	cpEGFP	62.2/16.8(160 AP)	144 nM	2.9	480 ms/1796 ms (10 AP)	2013	[16]
GCaMP6f (fast)	Ca^{2+}	CaM/M13	cpEGFP	50.8/13.14(160 AP)	375 nM	2.27	80 ms/400 ms (10 AP)	2013	[16]
jGCaMP7s (sensitive)	Ca^{2+}	CaM/M13	cpEGFP	39.42/4.7(160 AP)	68 nM	2.49	70 ms/1695 ms(10 AP)	2018	[63]
jGCaMP7f (fast)	Ca^{2+}	CaM/M13	cpEGFP	29.19/5.2(160 AP)	174 nM	2.3	75 ms/520 ms (10 AP)	2018	[63]
jGCaMP7b	Ca^{2+}	CaM/M13	cpEGFP	21.14/3.8(160 AP)	82 nM	3.06	80 ms/850 ms (10 AP)	2018	[63]
jGCaMP7c (contrast)	Ca^{2+}	CaM/M13	cpEGFP	144.6/12.1(160 AP)	298 nM	2.44	85 ms/900 ms (10 AP)	2018	[63]
XCaMPGf (fast)	Ca^{2+}	CaM/ckkap	cpEGFP	11.6/5.5(6 spikes)	115 nM	1.4	50 ms/140 ms (1 AP)	2019	[62]
XCaMP-R	Ca^{2+}	CaM/ckkap	cpApple	5.57/1.5(8 spikes)	97 nM	1.1	30 ms/200 ms (1AP)	2019	[62]
jRCaMP1a	Ca^{2+}	CaM/M13	cpmRuby	2.2/1.2(160 AP)	214 nM	0.86	150 ms/3500 ms (160AP)	2016	[25]
jRCaMP1b	Ca^{2+}	CaM/M13	cpmRuby	6.2/2.2(160 AP)	712 nM	1.6	300 ms/1500 ms (160AP)	2016	[25]
jRGECO1a	Ca^{2+}	CaM/M13	cpmApple	10.6/2.1(160 AP)	148 nM	1.9	100 ms/3000 ms (160AP)	2016	[25]
R-CaMP2	Ca^{2+}	CaM/ckkap	cpmApple	4.8/0.8 (6 spikes)	69 nM	1.2	55 ms/240 ms (1AP)	2015	[70]
K-GECO1	Ca^{2+}	CaM/ckkap	cpFusionRed	11/1(10 AP)	165 nM	1.12	120 ms/2700 ms(160AP)	2018	[69]
NIR-GECO1	Ca^{2+}	CaM/RS20	Split mIFP	-0.9/-0.5(160 AP)	215 nM	1.03	1250 ms/6500 ms (160AP)	2019	[23]
REX-GECO1	Ca^{2+}	CaM/M13	cpmApple	59[b]/3(150 Hz)	240 nM	1.8	ND/ND	2014	[75]
sPA-GCaMP6f[c]	Ca^{2+}	CaM/M13	cpEGFP	9/1.2(>10 AP)	650 nM	2.7	ND/ND	2015	[72]
CaMPARI (green)	Ca^{2+}	CaM/M13	cpmEos2	-0.88/ND	128 nM	2.4	ND/ND	2015	[73]
CaMPARI (red)	Ca^{2+}	CaM/M13	cpmEos2	-0.95/ND	74 nM	2.3	ND/ND	2015	[73]
CaMPARI2 (green)	Ca^{2+}	CaM/M13	cpmEos2	-0.88/ND	199 nM	ND	ND/ND	2018	[74]
CaMPARI2 (red)	Ca^{2+}	CaM/M13	cpmEos2	ND/ND	ND	ND	ND/ND	2018	[74]
GCaMP-X_c	Ca^{2+}	CaM/M13	cpEGFP	NA/0.25[d]	ND	ND	~120 ms/~650 ms[d]	2018	[24]

[a]τ < 10 ms for [Ca^{2+}] >500 nM. [b]ΔR/R, R=I_{450nm}/I_{580nm}. [c]Photoactivated form. [d]Single-AP like Ca^{2+} transients-induced signal. AP, action potential. ND, not determined.

4.2 Voltage indicators

Plasma membrane voltage changes are essential in neuron signal transmission. Current genetically encoded voltage indicators (GEVIs) are based on voltage sensitive domains (VSDs) and microbial rhodopsins, introduced by Micah S. Siegel *et al* (1997) and Joel M. Kralj *et al* (2011), respectively[53,76,77]. So far, all cpFP-based GEVIs are based on four-transmembrane VSDs that change their conformations upon trans-membrane voltage change (Table 3). Sunita Ghimire Gautam *et al* (2009) first tried to fuse green cpEGFP or red cpmKate to the intracellular C-terminus of the VSD of *Ciona intestinalis* voltage sensor-containing phosphatase (CiVSD) and only the red sensors gave modest sensitivity with slow kinetics[78]. To address this issue, Lauren Barnett *et al* (2012) fused a series of CT truncated CiVSD to the N-terminus of cpEGFP and screened out a probe named ElectricPK, which is the first cpFP GEVI with a fluorescence response fast enough to resolve multiple action potentials in mammalian neurons[79]. Following this design, Ahmed S. Abdelfattah *et al* (2016) used bacterial and mammalian cells to optimize the brightness and sensitivity of CiVSD-cpmApple, respectively, leading to red voltage probe called FlicR1 capable of tracking voltage oscillations at 100 Hz in dissociated hippocampal neurons[80]. Another breakthrough using the cpFP scaffold as a voltage reporter came from François St-Pierre *et al* (2014)[54]. Instead of the C-terminus of VSD, the extracellular S3-S4 loop of the *Gallus gallus* VSD (GgVSD) was inserted with cpsfGFP to generate the ASAP1 sensor with τ_{on}/τ_{off} of ~2 ms, which could track trains of action potential waveforms up to 200 Hz. Further directed protein evolution effort led to the better indicator ASAP3 (2018) with higher sensitivity and faster activation kinetics[48].

The ideal GEVIs should have sufficient brightness and photostability, decent plasma membrane trafficking, and sub-millisecond response kinetics, which are not required for the GECIs. Current GEVIs are inferior to the state-of-the-art GECIs, especially in sensitivity and brightness, limiting the ability of GEVIs to report neuronal activity *in vivo*[81].

Table 3 Summary of cpFP-based voltage sensors.

Indicator	Sensing module	cpFP	$\Delta F/F_0$ 1AP/per 100 mV[a]	τ_{on}, τ_{2on} /τ_{off}, τ_{2off} (ms)[b]	Applications	Year	Ref.
ElectricPK	CiVSD	cpEGFP	-0.7%/-1.2%	2.24, NA/2.09, 69.07	HEK293 cells; *in vitro* hippocampal neurons	2012	[79]
ASAP1	GgVSD	cpsfGFP	-5% /-17.5%	2.1, 71.5/2.0, 50.8	HEK293A cells; *in vitro* dissociated rat hippocampal neuron; cortical slices; dissociated hippocampal cultures	2014	[54]

ASAP3	GgVSD	cpsfGFP	-18%/-51%	0.94,7.24/ 3.79, 16[c]	Interneurons in acute cerebellar slices; acute brain slices; visual cortex of awake mice;layer-5 cortical neurons	2018	[48]
FlicR1	CiVSD	cpmApple	-3% /~10%	0.74,27/0.9, 14[c]	HEK293T cells; *in vitro* hippocampal neurons; organotypic rat hippocampal slices	2016	[80]

[a]The 100 mV change means from -70 mV to +30 mV. [b]Percentage of different components are not shown here. [c]Values were measured around 34°C. NA, not applicable.

4.3 Neurotransmitter indicators

Neurotransmitters are endogenous chemicals that are secreted by neurons and transmit signals to their target neurons or effector cells. Detecting the spatial-temporal distribution of neurotransmitters is the key to understand the chemical neurotransmission process. To date, two classes of sensitive cpFP indicators for neurotransmitters have been developed based on two kinds of sensing domains: bacterial periplasmic binding proteins (PBPs) and G protein-coupled receptors (GPCRs), first described by Loren L Looger lab (2013) and Yulong Li lab (2018)/Lin Tian lab (2018), respectively (Table 4)[5].

Jonathan S Marvin *et al* (2013) from Looger group reported glutamate sensor iGluSnFR with cpEGFP inserted into the interdomain hinge region of a bacterial PBP GltI[49]. iGluSnFR showed a $\Delta F/F_0$ of 4.5 and 1.03 on the plasma membrane of HEK293 cells and neurons, respectively, with an appropriate kinetics (τ_{on} ~ 5 ms, τ_{off} ~ 92 ms) that enables visualization of glutamate release from presynaptic terminals at frequencies up to 10 Hz. To improve the brightness and kinetics, the same group (2018) engineered a series of brighter iGlucSnFR variants with different affinities and kinetics by replacing cpEGFP with cpsfGFP and introducing mutations into the glutamate-binding pocket[82]. Two sensors SF-iGluSnFR.S72A and SF-iGluSnFR.A184S exhibited shorter rise and decay time than GCaMP6f (10.6 ms and 29.1 ms vs 111.4 ms of τ_{off}, respectively) in neuron buttons and successfully detected glutamate concentration changes upon 100 Hz stimulation. Interestingly, for iGluSnFR and its variants, the affinities were much higher (~10-fold) when expressed on the cell surface than the purified form. At the same time, Nordine Helassa *et al* introduced a single mutation (S72T) near the glutamate-binding site of iGluSnFR and also developed an ultrafast sensor $iGlu_u$ with τ_{off} of ~ 2.6 ms (vs τ_{off} of ~ 13.8 ms for iGluSnFR in neuron buttons), enabling imaging of glutamate clearance and synaptic depression during 100 Hz spike trains[83]. Using similar strategy, Looger group also developed cpFP sensors for other neurotransmitters such as GABA and Nicotine[84,85]. However, one big problem of this approach is that the availability of bacterial PBPs for neurotransmitters is limited. Moreover, their affinities and kinetics are probably not optimal for neurotransmitters in mammalian cells, thus requiring extensive protein engineering.

To overcome these drawbacks, Yulong Li group developed a series of neurotransmitter indicators called GPCR-activation-based sensors (GRAB sensors) using natural GPCRs. For dopamine, Fangmiao Sun *et al* (2018) from Li lab developed $GRAB_{DA1m}$ and $GRAB_{DA1h}$ indicators with different affinities (DA1m: EC_{50} =130 nM, $\Delta F/F_0$=0.9, τ_{on}/τ_{off}

= 60 ms/710 ms; DA1h: EC_{50} = 10 nM, $\Delta F/F_0$ = 0.9, τ_{on}/τ_{off} = 140 ms/2520 ms) by inserting the cpEGFP into the third intracellular loop (ICL3) of human dopamine D_2 receptor (D_2R), optimizing the insertion site and linkers, and introducing mutations associated with the affinity[46]. Both sensors have relatively high specificity for dopamine over similarly structured norepinephrine (NE) because of their ~10-fold higher affinity to dopamine. $GRAB_{DA}$ sensors enable rapid and specific detection of DA in a variety of living organisms including flies, zebrafish, mice and bird[46,86]. With a similar strategy, the same group (2019, 2018) employed α_2-adrenergic receptor and human muscarinic acetylcholine receptor M_3R as sensing domains and engineered two NE sensors (NE1m: $\Delta F/F_0$ = 2.3, τ_{on}/τ_{off} = 69 ms/750 ms, EC_{50} = 930 nM; NE1h: $\Delta F/F_0$ = 1.2, τ_{on}/τ_{off} = 29 ms/2000 ms, EC_{50} = 83 nM) and one acetylcholine sensor (GACh2.0: $\Delta F/F_0$ = 0.9, τ_{on}/τ_{off} = 280 ± 32 ms/762 ± 75 ms, EC_{50} = 700 nM)[87,88]. The NE1m/NE1h sensors have a ~350-fold/37-fold higher affinity to NE over dopamine, respectively.

At the same time, Lin Tian group (2018) developed dopamine indicators using the same strategy as GRAB sensors[89]. Based on human dopamine D_1 receptor (D_1R), the dLight1.1 indicator has a $\Delta F/F_0$ of 2.3 (K_d = 330 ± 30 nM) and a single F129A mutation in D_1R increased the dynamic range (dLight1.2, $\Delta F/F_0$ = 340 ± 20%, K_d = 770 ± 10 nM, τ_{on} = 9.5 ± 1.1 ms, τ_{off} = 90 ± 11 ms in brain slices). Further optimization of insertion site or replacing the D_1R with other GPCRs such as D_4R and D_2R, led to various versions of dLights with different dynamic ranges and affinities. These authors also verified their design strategy in other GPCRs and hence provided a platform for developing indicators for other neurotransmitters.

Interestingly, all reported GPCR-based neurotransmitter indicators have undetectable or negligible coupling to downstream signaling events compared to the wild type GPCRs. Instead, the fluorescence readout seems to be the only downstream event of these sensors, allowing more accurate interrogation of neurotransmitter dynamics with minimal perturbation to the cell physiology. Furthermore, the amplitude of the response to the pharmacological compound reflected the efficacy of drugs on the wild-type receptors, which could be useful for screening of GPCR activators or inhibitors[87,89].

Table 4 Summary of cpFP-based neurotransmitter sensors.

Indicator	Analyte	Sensing module	FP	$\Delta F/F_0$ *in vivo*	K_d *in vivo*	τ_{on}/τ_{off} or k_{on}/k_{off} ($\mu M^{-1}s^{-1}/s^{-1}$)	Year	Ref.
iGluSnFR	Glutamate	GltI	cpGFP	1-4	4 μM	15 ms/92 ms (1AP)	2013	[49]
SF-iGluSnFR(A184V)	Glutamate	GltI	cpsfGFP	1.0	2.1μM	5/52	2018	[82]
SF-iGluSnFR(S72A)	Glutamate	GltI	cpsfGFP	2.5	34 μM	0.6/108	2018	[82]
SF-iGluSnFR(A184S)	Glutamate	GltI	cpsfGFP	0.7	0.6 μM	6/25	2018	[82]

$iGlu_f$	Glutamate	GltI	cpEGFP	1.0	26 μM	ND/5.2 ms	2018	[83]
$iGlu_u$	Glutamate	GltI	cpEGFP	1.7	53 μM	ND/2.6 ms	2018	[83]
iNicSnFR3a	Nicotine	OpuBC	cpsfGFP	2.5-4.5	~20 μM	0.07/2.0	2019	[84]
iGABASnFR	GABA	Pf622	cpsfGFP	2.5	9 μM	ND/ND	2018	[85]
$GRAB_{DA1m}$	Dopamine	D_2R	cpEGFP	0.9	130 nM	60 ms/0.7 s	2018	[46]
$GRAB_{DA1h}$	Dopamine	D_2R	cpEGFP	0.9	10 nM	140 ms/2.5 s	2018	[46]
dLight1.1	Dopamine	D_1R	cpEGFP	2.3	330 nM	ND/ND	2018	[89]
dLight1.2	Dopamine	D_1R	cpEGFP	3.4	770 nM	9.5 ms/90 ms	2018	[89]
$GRAB_{NE1m}$	Norepinephrine	α_2AR	cpEGFP	2.3	930 nM	72 ms/680 ms	2019	[88]
$GRAB_{NE1h}$	Norepinephrine	α_2AR	cpEGFP	1.3	83 nM	36 ms/1890 ms	2019	[88]
GACh2.0	Acetylcholine	M_3R	cpGFP	1.0	0.78 μM	280 ms/762 ms	2018	[87]

4.4 Redox state-related indicators

Cellular redox states are important for cell metabolism and regulated by many chemicals, such as the NADPH/$NADP^+$ pair, NADH/NAD^+ pair, reactive oxygen species (ROS), reactive nitrogen species (RNS), cysteine/cysteine (Cys/Cys) redox couple and glutathione redox couple[90-92].

The first NADH sensor Frex and its variant FrexH with high affinity (K_d ~ 3.7 μM/40 nM *in vitro*, respectively) were reported by Yuzheng Zhao *et al* (2011) (Table 5)[93]. In Frex and FrexH, cpYFP are sandwiched by two B-Tex sensing domains and they are only sensitive to NADH rather than NAD^+, NADPH, $NADP^+$, ATP or ADP, with a $\Delta F/F_0$ of 8 *in vitro*. Live-cell imaging with these sensors showed that the concentration of NADH in the cytosol and mitochondria of HEK293T cells is ~ 130 nM and ~ 30 μM, respectively, suggesting different roles for NADH in different organelles. Meanwhile, Yin Pun Hung *et al* (2011) developed the first NADH/NAD^+ sensor named Peredox ($\Delta F/F_0$ ~ 1.5) by placing cpT-Sapphire between two T-Rex sensing domains and optimizing the pH stability and kinetics[92]. Peredox's affinities to NADH and NAD^+ are too high and the dynamic range is limited. To overcome these issues, Yuzheng Zhao *et al* (2015) engineered another NADH/NAD^+ sensor named SoNar with a different design where cpYFP was inserted into single T-Rex domain[64]. SoNar has appropriate affinities for NADH and NAD^+ (K_d ~ 0.2 μM and 5 μM *in vitro*, respectively) and is highly sensitive for the NADH/NAD^+ ratio with a $\Delta R/R_0$ of 14 ($R = I_{420nm}/I_{485nm}$) even in the presence of $NADP^+$, NADPH, ATP or ADP. With this probe, several compounds affecting cancer cell metabolism and viability were screened out. In addition, starting with SoNar, the same group (2017) developed NADPH sensors called iNaps with different affinities through mutations of the binding pocket of SoNar[40]. Like their precursor, iNaps are ratiometric

sensors with large dynamic range and high selectivity. An NAD^+-specific cpFP sensor with a $\Delta F/F_0$ of -0.5 was introduced by Xiaolu A. Cambronne *et al* (2016)[94], in which the authors inserted cpVenus into an NAD^+-binding domain from a bacterial DNA ligase while abolishing the enzyme activity.

cpFP sensors for ROS/RNS including superoxide (O_2-), organic hydroperoxide (OHP) and hydrogen peroxide (H_2O_2), and their oxidized product methionine sulfoxide (MetO) have also been extensively explored (Table 5). Wang Wang *et al* (2008) first described that cpYFP itself is sensitive to superoxide ($\Delta F/F_0$ ~4) and could monitor superoxide flashes in mitochondria[95]. However, cpYFP is also sensitive to hydroxyl radical (-OH) and nitric oxide (NO)[95]. Boxuan Simen Zhao *et al* (2010) developed an organic hydroperoxide indicator called OHSer by inserting cpVenus into bacterial Xc-OhrR[96]. OHser showed small or negligible signal changes toward other ROS molecules such as H_2O_2, -OCl, O_2- or NO. H_2O_2 is an important signal molecule in the cell and of general interest for biological researchers. Vsevolod V Belousov *et al* (2006) developed the first cpFP H_2O_2 sensor named HyPer by inserting cpYFP into the regulatory domain of bacterial OxyR (Oxy-RD)[97]. HyPer showed extremely high selectivity to H_2O_2 over other ROS molecules such as O_2-/GSSG/NO/ONOO-. Interestingly, HyPer's dimeric variants HyPer-2 showed expanded dynamic range ($\Delta R/R_0$ ~ 5 vs $\Delta R/R_0$ ~ 2 for HyPer)[98]. However, the kinetics was slow. Further mutations in the OxyR dimerization interface led to HyPer-3 combining the advantages of fast kinetics of HyPer and large dynamic range of HyPer-2[99]. To facilitate multi-color imaging, Yulia G. Ermakova *et al* (2014) developed a spectrally distinct red-shifted H_2O_2 sensor HyPerRed[100]. In cells, the above ROS can convert methionine to the S and R diastereomers of MetO (MetSO and MetRO). MetO is a relatively stable molecule and could be a useful redox marker. Lionel Tarrago *et al* (2015) made sensors for MetSO and MetRO by fusing two ends of cpYFP with the methionine sulfoxide reductase A or B and thioredoxin 1 or thioredoxin 3, respectively, and demonstrated their applications in *E.coli* and HEK293 cells[101].

Besides the FP mutants, cpFPs were also used to develop indicators for measuring thiol/disulfide status, which is also an important redox pair in cells (Table 5) [90,102-105]. Yichong Fan *et al* (2015) developed redox-sensitive red fluorescent protein 1 (rxRFP1) by introducing cysteine pair to the two termini of cpmApple and optimizing the residues near them[106]. Later, by coupling the active-site cysteine residues of Trx1 with the cysteine pair at the termini of rxRFP1, Yichong Fan *et al* (2017) developed TrxRFP1 sensor to monitor thioredoxin redox status in living cells[91].

Table 5 Summary of cpFP-based sensors for ROS and redox states.

Indicator	Analyte	Sensing module	FP	$\Delta F/F_0$ or $\Delta R/R_0$	K_d/EC_{50}	τ_{on}/τ_{off} or k_{on}/k_{off} ($\mu M^{-1}s^{-1}/s^{-1}$)	Year	Ref.
Frex	NADH	B-Rex	cpYFP	9	3.7 μM	ND/ND	2011	[93]

FrexH	NADH	B-Rex	cpYFP	-0.75	40 nM	ND/ND	2011	[93]
Peredox	NAD^+/NADH	T-Rex	cpT-Sapphire	1.5	ND	ND/16 s	2011	[92]
SoNar	NAD^+/NADH	T-Rex	cpYFP	14[a]	5 μM (NAD^+), 0.2 μM (NADH)	ND/ND	2015	[64]
iNaps	NADPH	T-Rex	cpYFP	8[a]	2,6,25,120μM[b]	ND/ND	2017	[40]
NAD+ biosensor	NAD^+	NAD^+-binding domain from bacterial DNA ligase	cpVenus	-0.5	65 μM	ND/ND	2016	[94]
HyPer	H_2O_2	*E. Coli* OxyR-RD	cpYFP	~2[a]	160 nM	10 s/200 s	2006	[97]
HyPer-2	H_2O_2	*E. Coli* OxyR-RD	cpYFP	4.2-5[a]	290 nM	30 s/300 s	2011	[98]
HyPer-3	H_2O_2	*E. Coli* OxyR-RD	cpYFP	4.5[a]	260 nM	20 s/110 s	2013	[99]
HyPerRed	H_2O_2	*E. Coli* OxyR-RD	cpmApple	1.0	140 nM	ND/~300 s	2014	[100]
OHSer	OHP(Organic Hydroperoxide)	Bacterial Xc-OhrR	cpVenus	0.8	ND	ND/ND	2010	[96]
cpYFP	Superoxide(O_2-)	cpYFP	cpYFP	3.2	ND	ND/ND	2008	[95]
MetSOx	MetSO	MSRA and Trx1	cpYFP	3	1 μM[c]	ND/ND	2015	[101]
MetROx	MetRO	MSRB and Trx3	cpYFP	-0.61	0.5 μM[c]	ND/ND	2015	[101]
rxRFP1	Oxidant/reductant	Cysteine residues pair (Reversible disulfide bridges)	cpmApple	~3.0	ND	ND/ND	2015	[106]
TrxRFP1	Thioredoxin (Trx)	Cysteine residues pair (Reversible disulfide bridges)/Trx1	cpmApple	~5.0	27 nM[d]	~60 s/~30 s	2017	[91]

[a]$\Delta R/R_0$. [b]These affinities are for iNap1, iNap2, iNap3, iNap4, respectively. [c]For MetO in proteins. [d]For H_2O_2 stimulation, assuming 500 fold decrease in intracellular H_2O_2 concentration compared to medium.

4.5 Second messenger indicators

Second messengers are molecules that relay the signals from cell-surface receptors to the intracellular downstream effectors. Second messengers include cAMP, cGMP, calcium, IP3, DAG and so on. For cAMP indicators, several different groups have tried different sensing domains from mammalian cells and different FPs including Citrine/GFP/mNeonGreen/mApple, and already developed sensors with different dynamic ranges, affinities, and brightness (Table 6)[17,18,43,107-109]. For cGMP indicators, based on different cGMP-binding domains, Lydia W. M. Nausch *et al* (2008) and Shogo Matsuda *et al* (2017) developed green cGMP sensors δ-FlincG and Green cGull, respectively (Table 6)[19,110]. However, large dynamic range and high brightness are not compatible in the above-mentioned sensors expressed in mammalian cells at 37°C. Furthermore, current cAMP cpFP sensors have only ~ 10-fold higher affinity than

cGMP and should be improved for simultaneous cAMP/cGMP imaging.

DAG and Ins(1,3,4,5)P_4, are also important messengers in the cell. Paul Tewson *et al* (2012) reported several downward and upward DAG sensors having PKCδ isoform incorporated with cpGFP[111]. To improve dynamic range and brightness, Paul Tewson *et al* (2013, 2016) performed mutagenesis and substitution of cpGFP with cpmNeonGreen, which was derived from the brightest and a rapidly-maturing monomeric green FP mNeonGreen[107,112]. For Ins (1,3,4,5)P_4, Reiko Sakaguchi *et al* (2009) developed a cpFP sensor with cpGFP placed in the Btk PH domain[113].

Table 6 Summary of cpFP-based sensors for second messengers, key metabolites, ions, kinases and transporters.

Indicator	Analyte or activity	Sensing domain	FP	$\Delta F/F_0$ ($\Delta R/R_0$)	K_d	τ_{on}/τ_{off} or k_{on}/k_{off} ($\mu M^{-1}s^{-1}/s^{-1}$)	Application	Year	Ref.
Flamindo2	cAMP	mEpac1 regulatory domain	Split Citrine	-0.75	3.2 μM	ND/ND	COS7 cells; HeLa cells	2014	[18]
cAMPr	cAMP	mPKA-catalytic domain and bPKA regulatory domain	cpGFP	0.6	ND	ND/ND	Embryonic stem (ES) cells; SAG-differentiated neurons; *Drosophila* brains	2018	[43]
cADDis	cAMP	mEpac2	cpmNeonGreen	-0.55	>10 μM	ND/ND	HEK293T cells	2016	[107]
R-FlincA	cAMP	rPKA-RIα-regulatory domain	cpmApple	7.6	0.3 μM	ND/ND	HEK293T cells; *D. discoideum* cells; MIN6 cells	2018	[109]
Pink Flamindo	cAMP	mEpac1 regulatory domain	Split mApple	3.2	7.2 μM	<5 s/ND	HeLa cells; MIN6 m9 cells; cerebral cortical astrocytes	2017	[108]
δ-FlincG	cGMP	PKGIα	cpEGFP	0.75	170 nM	120 ms/160 ms	VSM cells	2008	[110]
Green cGull	cGMP	PDE5α cGMP-binding domain	Split Citrine	6.5	1.09 μM	ND/ND	HEK293/ GLUTag/C6/COS 7 cells	2017	[19]
Upward DAG	DAG	PKCδ	cpEGFP	0.45	ND	ND/ND	HEK293 cells	2012	[111]
Upward DAG2	DAG	PKCδ	cpEGFP	~1	ND	ND/ND	HEK293 cells	2013	[112]
Upward DAG3	DAG	PKCδ	cpmNeonGreen	0.48	ND	ND/ND	HEK293T cells	2016	[107]
Ins(1,3,4,5)P_4 sensor	Ins(1,3,4,5)P_4	Human Btk PH domain	cpGFP	0.5	1 μM	ND/ND	ND	2009	[113]
Perceval	ATP/ADP	GlnK1	cpmVenus	1[a]	0.5(K_R)	ND/ND	HEK293 cells	2009	[114]
PercevalHR	ATP/ADP	Bacterial protein GlnK1	cpmVenus	>7[a]	3.5(K_R)	ND/ND	Cultured mouse embryonic cortical neurons; cultured astrocytes; HEK293 cells; Neuro2A neuroblastoma cells	2013	[115]
MalionG	ATP	ε subunit of F_0F_1-	Split Citrine	3.9	1.1 mM	12/0.095	Brown adipocytes; HeLa cells	2018	[20]

MalionB	ATP	ATP synthase ε subunit of F_0F_1-ATP synthase	Split BFP	0.9	0.46 mM	31/0.015	Brown adipocytes; HeLa cells	2018	[20]
MalionR	ATP	ATP synthase ε subunit of F_0F_1-ATP synthase	Split mApple	3.5	0.34 mM	25/0.016	Brown adipocytes; HeLa cells	2018	[20]
QUEEN-7μ	ATP	ATP synthase ε subunit of F_0F_1-ATP synthase	cpEGFP	4[a]	7.2 μM	ND/ND	*E. coli* cells	2014	[116]
QUEEN-2m	ATP	ATP synthase ε subunit of F_0F_1-ATP synthase	cpEGFP	3.5[a]	4.5 mM	ND/ND	*E. coli* cells	2014	[116]
iATPSnFR1.0	ATP	ATP synthase ε subunit of microbial F_0F_1-ATP synthase	cpsfGFP	2.4	350-630 μM	~2.5 s/~2 s	HEK293T cells; astrocytes; neurons	2019	[117]
iATPSnFR1.1	ATP	ATP synthase ε subunit of microbial F_0F_1-ATP synthase	cpsfGFP	1.9	138 μM	<1.5 s/<1.5 s	HEK293T cells; astrocytes; neurons	2019	[117]
GEVAL30	GTP	G protein domain of FeoB	cpYFP	3	33.2 μM	ND/ND	SK-Mel-103 human melanoma cells; high-throughput (HTP) screening	2017	[118]
mOGsor	2OG	NifA GAF domain	Split YFP	1.5	62.4 mM	ND/ND	*E.coli* cells	2014	[119]
Citrate sensor (CF98)	Citrate	CitAP	cpGFP	0.6	2 mM	<1 ms/ND	*E. coli* cells	2013	[120]
FHisJ	Histidine	HisJ	cpYFP	4.2[a]	22 μM	ND/ND	HeLa cells	2017	[121]
$FGBP_{1\ mM}$	Glucose	GGBP	cpYFP	5.9[a]	1 mM	ND/ND	*E. coli* JM109 (DE3) cells	2018	[122]
Green Glifons	Glucose	MglB	Split Citrine	6	50-4000 μM	ND/ND	Mouse blood samples; HeLa cells; pharyngeal muscle of *C. elegans*; mouse pancreatic MIN6 m9 β cells	2019	[21]
iGlucoSnFR	Glucose	*T. thermophilus* GBP	cpGFP	2.3	7.7 mM	0.000031/0.38	HEK293T cells; rat astrocytes and neurons; *Drosophila*; zebrafish larvae	2019	[123]
EcPhnD90-cpGFP.L1ADΔΔ.L297R/L301R	Pn (-O_3P-R)	EcPhnD	cpGFP	1.6	~20 μM	ND/ND	ND	2011	[124]
MBP165-cpGFP.PPYF	Maltose	*E. coli* maltose-binding protein (MBP)	cpGFP	1.5	3 μM	ND/ND	HEK293 cells	2011	[13]
GZnP1	Zn^{2+}	ZF1 and ZF2 from Zap1	cpGFP	1.6	58 pM	ND/ND	HeLa cells	2016	[125]

GZnP2	Zn^{2+}	ZF1 and ZF2 from Zap1	cpGFP	5/3.5	352 pM	ND/ND	HeLa/Cos-7/HEK293/INS-1 cells	2018	[126]
GINKO1	K^+	Bacterial K+ binding protein	Split EGFP	3.3[a]/	0.42 mM	9320/85.9	Neurons; glial cells	2019	[22]
Green-sinphos	Insulin receptor activation	IRS-1 substrate domain and SH2n of p85	cpEGFP	0.15	ND	ND/ND	CHO cells	2004	[127]
ExRai-AKAR	PKA activity	PKA substrate and FHA1 domain of AKAR	cpEGFP	1.86[a]	ND	ND/ND	HeLa cells; PC12 cells	2018	[9]
ExRai-CKAR	PKC activity	PKC substrate and FHA1 domain of AKAR	cpEGFP	1.56[a]	ND	ND/ND	HeLa cells	2018	[9]
ExRai-AktAR	Akt/PKB activity	Akt substrate and FHA1 domain of AKAR	cpEGFP	0.93[a]	ND	ND/ND	NIH3T3 cells	2018	[9]
GphosEphB	EphB activity	EphB2 substrate and SH2 domain of Fyn	cpEGFP	0.2	ND	ND/ND	HEK293T cells; neurons	2018	[128]
GphosEphA	EphA activity	EphA4 substrate and SH2 domain of Fyn	cpEGFP	0.4	ND	ND/ND	HEK293T cells; neurons	2018	[128]
AmTrac	NH_4^+ channel activity	Arabidopsis thaliana AMT1;3	cpGFP	-0.3	55 µM	ND/ND	Yeast	2013	[129]
AmTrac-LS	NH_4^+ channel activity	Arabidopsis thaliana AMT1;3	cpGFP	-0.3	55 µM	ND/ND	Yeast	2013	[129]
deAmTrac-CP	NH_4^+ channel activity	Arabidopsis thaliana AMT1;3	cpGFP	1[b]	54 µM	ND/ND	Yeast	2015	[130]
deAmTrac-FP	NH_4^+ channel activity	Arabidopsis thaliana AMT1;3	cpGFP	0.83[b]	36 µM	ND/ND	Yeast	2015	[130]

[a]Excitation ratio. [b]Emission ratio. K^R, the ratio of [ATP] to [ADP].

4.6 Metabolite indicators

Metabolites are the intermediates and products of metabolic reactions catalyzed by various enzymes in cells, and are usually restricted to small organic and inorganic molecules including ATP and ADP (Table 6).

The ATP:ADP ratio is a critical parameter of cellular energy status that regulates many metabolic activities. Jim Berg *et al* (2009) inserted cpmVenus into the T loop of GlnK1

from *Methanococcus jannaschii* to make ATP/ADP sensor Perceval[114]. To obtain larger dynamic range, Mathew Tantama *et al* (2013) mutated the residues near the binding pocket of Perceval and screened a variant called PercevalHR with a $\Delta R/R_0$ of 7 and expanded sensing range for ATP/ADP ratio[115].

Sensors with high selectivity toward ATP over ADP are also highly desired. Satoshi Arai *et al* (2018) developed blue/green/red ATP indicators named MaLionB/G/R by inserting the ε subunit of the ATP-binding region of bacterial F_0F_1-ATP synthase into FP variants of different colors[20]. These sensors showed minimal signal changes toward other molecules such as ADP/AMP/dATP/GTP. In addition, Mark A. Lobas *et al* (2019) developed ATP sensors iATPSnFRs with similar or higher affinities than MaLions and demonstrated their use in astrocytes and neurons[117]. When targeting to plasma membrane, the affinity and dynamic range of iATPSnFRs decreased (purified iATPSnFR1.0: $\Delta F/F_0$ = 2.4, EC_{50} = 120 μM vs pm iATPSnFR1.0: $\Delta F/F_0$ = 1.0, EC_{50} = 350 μM; purified iATPSnFR1.1: $\Delta F/F_0$ = 1.9, EC_{50} = 50 μM vs pm iATPSnFR1.1: $\Delta F/F_0$ =0.88, EC_{50} = 138 μM. pm, plasma membrane).

cpFP sensors for other metabolites, such as GTP, 2-Oxoglutarate (2OG), citrate, histidine, glucose, maltose and phosphonate (Pn, $-O_3P-R$), have also been reported. Anna Bianchi-Smiraglia *et al* (2017) inserted cpYFP into the loop of bacterial iron-transport protein FeoB and obtained a series of ratiometric GTP sensors GEVALs with different affinities and dynamic ranges[118]. Chang Zhang *et al* (2014) and Yuki Honda *et al* (2013) generated a 2OG sensor mOGsor and a citrate indicator, respectively, and further testing in mammalian cells is needed[119,120]. Hanyang Hu *et al* (2017) generated a ratiometric histidine sensor named FHisJ by inserting cpYFP into a type II periplasmic binding protein HisJ[121]. However, the high affinity for histidine reduces the sensitivity of FHisJ in mammalian cells. Glucose is a main energy source in human and its dysregulation is a hallmark of diabetes. Three different groups developed different cpFP glucose indicators for particular applications. Hanyang Hu *et al* (2018) generated indicators for glucose by inserting cpYFP into the flexible linker regions of bacterial periplasmic protein GGBP and monitored glucose transport in living *E. coli* cells[122]. Later, Marie Mita *et al* (2019) developed a series of glucose indicators named Green Glifons with different affinities by inserting bacterial D-galactose-binding periplasmic protein (MglB) into Citrine and demonstrated their use in live mammalian cell imaging[21]. Jacob P. Keller *et al* (2019) from Looger group also developed a series of glucose sensors with high SNR, fast kinetics and affinities varying over four orders of magnitude (1 μM to 10 mM) based on glucose-binding PBP (GBP) from the *thermophile T. thermophiles* and demonstrated their use in astrocytes, neurons and fruit fly/ larval zebrafish brains[123]. Looger group also developed cpFP indicators for maltose and Pn based on bacterial PBPs[13,124].

4.7 Ion indicators

Ions such as zinc (Zn^{2+})/potassium (K^+) are important components of the cell system and regulate many signal pathways. Yan Qin *et al* (2016) developed a green Zn^{2+} probe GZnP1 by attaching two zinc fingers of the yeast transcription factor Zap1 (ZF1 and ZF2) to the two ends of cpGFP and optimizing the Zn^{2+} sensing domain and linkers using

rational and computational protein design[125]. Further screening on GZnP1 resulted in GZnP2 (2018) with a 2-fold larger dynamic range ($\Delta F/F_0 \sim 5$)[126].

Potassium ions (K^+) are essential for maintaining a normal cell resting membrane potential and for generating and propagating APs in neurons. Soon after the bacterial K^+-binding protein (Kbp) was reported, Yi Shen *et al* (2019) first reported a cpFP K^+ sensor GINKO1, which has bacterial K^+-binding domain Kbp placed within EGFP[22,131]. GINKO1, in conjunction with red calcium sensor K-GECO1, enabled dual-color imaging of K^+ and Ca^{2+} dynamics in the same neurons upon glutamate treatment.

4.8 Kinase indicators

Besides small molecules, cpFP indicators can also report protein activity such as kinase activity. In the past 20 years, researchers developed many FRET sensors for imaging enzyme activities in living cells as FRET-based sensor engineering is easier and more efficient[9,132]. However, cpFP-based sensors can be more sensitive than FRET-based sensors and more convenient for multi-event imaging. Yasutoshi Kawai *et al* (2004) developed cpFP indicators for monitoring insulin receptor kinase activation by connecting two ends of cpFP with a substrate peptide of the insulin receptor kinase and a phosphorylation recognition domain[127]. Using the same strategy, Sohum Mehta *et al* (2018) made cpFP indicators with different colors and large dynamic ranges for monitoring PKA/PKB/PKC activities in living cells[9]. Meanwhile, Yu-Ting Mao *et al* (2018) developed cpEGFP sensors for imaging the dynamics of EphA/EphB signaling in cortical neurons[128].

4.9 Membrane transporter indicators

Visualization of activities of other proteins, such as the membrane transport proteins that assist the movement of ions, small organic molecules, peptides and even macromolecules across a biological membrane, is highly desired. Roberto De Michele *et al* (2013) inserted cpGFP into the intracellular loop of the *Arabidopsis* ammonium transporter AMT1;3 to develop the AmTrac sensor that can report activity of ammonium transporter in living yeasts[129]. AmTrac is reversible, has a $\Delta F/F_0$ of - 0.25 and higher selectivity toward NH_4^+ over other ions. Further screening of the first linker resulted in AmTrac-LS with better brightness and signal change. The same group (2015) re-optimized the first linker of AmTrac and developed a set of dual-emission AmTrac sensors named deAmTracs with a $\Delta R/R_0$ of 1[130].

5. Future directions

cpFP indicators feature unique large sensitivity and fast kinetics, thereby rendering them particularly useful in neuroscience. However, some cpFP sensors still suffer from low sensitivity, low brightness, or slow kinetics, etc., and thus require further optimization. For example, the response measured by ASAP3, the most sensitive cpFP-based voltage sensor, has only 18% fluorescence change per AP. More sensitive variants could be

achieved by either extensive mutagenesis of the sensor, usage of brighter green FPs such as mNeonGreen (2.7-fold brighter than EGFP), or utilization of new voltage sensing domains. In addition, cpFP sensors for some key molecules in living cells are still lacking, such as second messenger 2'3'-cGAMP, which is associated with innate immune responses[133].

Compared to green cpFP indicators, the number of red/NIR ones is very limited, especially sensors for voltage, neurotransmitters, and kinases. Very recently, red cpFusionRed and NIR mIFP have demonstrated their utilities in calcium sensors, offering possibilities to engineer red-shifted cpFP sensors. However, both cpFP indicators have poor folding and/or low brightness, which could be improved by structure-guided mutagenesis or by use of brighter FPs. For example, NIR FP miRFP713 derived from bacteriophytochrome *Rp*BphP2 has 51% higher molecular brightness than mIFP from bacteriophytochrome *Br*BPhP. Starting with these new FPs, high-performance cpFP sensors with long-wavelength emission including voltage indicators could be engineered.

Super-resolution microscopy has overcome the diffraction limit of light in fluorescence imaging and enables visualization of fine spatial structures previously unseen. Given the unique ability of cpFP sensors to detect changes in molecule concentration and activity, an obvious question arises: can these methods be combined to visualize cellular biochemical activity architecture with high spatio-temporal resolution? Indeed, recently, BiFC-based and FLINC-based stochastic optical fluctuation imaging (SOFI) techniques were developed to visualize protein-protein interactions or kinase activities with super-spatial resolution in living cells[12,134]. However, these methods either cannot monitor the association/disassociation of protein complexes or have low temporal resolution. The newly developed grazing incidence structured illumination microscopy (GI-SIM) and Hessian structured illumination microscopy (Hessian-SIM) enable time-lapse imaging with a spatiotemporal resolution of ~90 nm and ~3.7-5.3 ms[135,136]. With high-performance cpFP sensors, these imaging tools will open up a new window to explore complex signaling pathways in cells.

In conclusion, despite great progress in the development of cpFP sensors, there is still large room for improvement, especially for red FPs themselves and related sensors. With new sensing domains and high-throughput screening platforms, more high-performance sensors will be realized in future.

Acknowledgements

The authors would like to acknowledge the following funding: National Key Research and Development Program of China (2017YFA0700403), National Natural Science Foundation of China (Grant 31670872, 21874145, 2018M633180), Shenzhen Science and Technology Innovation Committee (KQJSCX20170331161420421, JCYJ20170818163925063, JCYJ20170818164040422, GJHS20170314160302802), Chinese Academy of Sciences (GJJSTD20180002). We also thank Drs. Michael Lin at Stanford University and Yulong Li at Peking University for the critical reading of this

manuscript, and Emily Wang from Harvard University for proofreading this manuscript.

Author Contributions

W. L., M. D., C.Y., L.W. and J.C. wrote the paper. All authors helped with the figure and table preparation.

References

1. Lin MZ, Schnitzer MJ: **Genetically encoded indicators of neuronal activity**. *Nat Neurosci* 2016, **19**:1142-1153.
2. Rodriguez EA, Campbell RE, Lin JY, Lin MZ, Miyawaki A, Palmer AE, Shu X, Zhang J, Tsien RY: **The Growing and Glowing Toolbox of Fluorescent and Photoactive Proteins**. *Trends Biochem Sci* 2017, **42**:111-129.
3. Bajar BT, Wang ES, Zhang S, Lin MZ, Chu J: **A Guide to Fluorescent Protein FRET Pairs**. *Sensors (Basel)* 2016, **16**.
4. Combs CA, Shroff H: **Fluorescence Microscopy: A Concise Guide to Current Imaging Methods**. *Curr Protoc Neurosci* 2017, **79**:2 1 1-2 1 25.
5. Wang H, Jing M, Li Y: **Lighting up the brain: genetically encoded fluorescent sensors for imaging neurotransmitters and neuromodulators**. *Curr Opin Neurobiol* 2018, **50**:171-178.
6. Miesenbock G, De Angelis DA, Rothman JE: **Visualizing secretion and synaptic transmission with pH-sensitive green fluorescent proteins**. *Nature* 1998, **394**:192-195.
7. Wang F, Niu W, Guo J, Schultz PG: **Unnatural amino acid mutagenesis of fluorescent proteins**. *Angew Chem Int Ed Engl* 2012, **51**:10132-10135.
8. Chen ZJ, Ai HW: **A highly responsive and selective fluorescent probe for imaging physiological hydrogen sulfide**. *Biochemistry* 2014, **53**:5966-5974.
9. Mehta S, Zhang Y, Roth RH, Zhang JF, Mo A, Tenner B, Huganir RL, Zhang J: **Single-fluorophore biosensors for sensitive and multiplexed detection of signalling activities**. *Nat Cell Biol* 2018, **20**:1215-1225.
10. Romei MG, Boxer SG: **Split Green Fluorescent Proteins: Scope, Limitations, and Outlook**. *Annu Rev Biophys* 2019, **48**:19-44.
11. Kim J, Lee S, Jung K, Oh WC, Kim N, Son S, Jo Y, Kwon HB, Do Heo W: **Intensiometric biosensors visualize the activity of multiple small GTPases in vivo**. *Nat Commun* 2019, **10**:211.
12. Mo GC, Ross B, Hertel F, Manna P, Yang X, Greenwald E, Booth C, Plummer AM, Tenner B, Chen Z, et al.: **Genetically encoded biosensors for visualizing live-cell biochemical activity at super-resolution**. *Nat Methods* 2017, **14**:427-434.
13. Marvin JS, Schreiter ER, Echevarria IM, Looger LL: **A genetically encoded, high-signal-to-noise maltose sensor**. *Proteins* 2011, **79**:3025-3036.
14. Molina RS, Qian Y, Wu J, Shen Y, Campbell RE, Drobizhev M, Hughes TE: **Understanding the Fluorescence Change in Red Genetically Encoded Calcium Ion Indicators**. *Biophys J* 2019, **116**:1873-1886.
15. Nakai J, Ohkura M, Imoto K: **A high signal-to-noise Ca(2+) probe composed of a single green fluorescent protein**. *Nat Biotechnol* 2001, **19**:137-141.
16. Chen TW, Wardill TJ, Sun Y, Pulver SR, Renninger SL, Baohan A, Schreiter ER, Kerr RA, Orger MB, Jayaraman V, et al.: **Ultrasensitive fluorescent proteins for imaging neuronal activity**. *Nature* 2013, **499**:295-300.
17. Kitaguchi T, Oya M, Wada Y, Tsuboi T, Miyawaki A: **Extracellular calcium influx activates adenylate cyclase 1 and potentiates insulin secretion in MIN6 cells**. *Biochem J* 2013, **450**:365-373.
18. Odaka H, Arai S, Inoue T, Kitaguchi T: **Genetically-encoded yellow fluorescent cAMP indicator**

with an expanded dynamic range for dual-color imaging. *PLoS One* 2014, **9**:e100252.
19. Matsuda S, Harada K, Ito M, Takizawa M, Wongso D, Tsuboi T, Kitaguchi T: **Generation of a cGMP Indicator with an Expanded Dynamic Range by Optimization of Amino Acid Linkers between a Fluorescent Protein and PDE5alpha**. *ACS Sens* 2017, **2**:46-51.
20. Arai S, Kriszt R, Harada K, Looi LS, Matsuda S, Wongso D, Suo S, Ishiura S, Tseng YH, Raghunath M, et al.: **RGB-Color Intensiometric Indicators to Visualize Spatiotemporal Dynamics of ATP in Single Cells**. *Angew Chem Int Ed Engl* 2018, **57**:10873-10878.
21. Mita M, Ito M, Harada K, Sugawara I, Ueda H, Tsuboi T, Kitaguchi T: **Green Fluorescent Protein-Based Glucose Indicators Report Glucose Dynamics in Living Cells**. *Anal Chem* 2019, **91**:4821-4830.
22. Shen Y, Wu SY, Rancic V, Aggarwal A, Qian Y, Miyashita SI, Ballanyi K, Campbell RE, Dong M: **Genetically encoded fluorescent indicators for imaging intracellular potassium ion concentration**. *Commun Biol* 2019, **2**:18.
23. Qian Y, Piatkevich KD, Mc Larney B, Abdelfattah AS, Mehta S, Murdock MH, Gottschalk S, Molina RS, Zhang W, Chen Y, et al.: **A genetically encoded near-infrared fluorescent calcium ion indicator**. *Nat Methods* 2019, **16**:171-174.
24. Yang Y, Liu N, He Y, Liu Y, Ge L, Zou L, Song S, Xiong W, Liu X: **Improved calcium sensor GCaMP-X overcomes the calcium channel perturbations induced by the calmodulin in GCaMP**. *Nat Commun* 2018, **9**:1504.
25. Dana H, Mohar B, Sun Y, Narayan S, Gordus A, Hasseman JP, Tsegaye G, Holt GT, Hu A, Walpita D, et al.: **Sensitive red protein calcium indicators for imaging neural activity**. *Elife* 2016, **5**.
26. Zhao Y, Araki S, Wu J, Teramoto T, Chang YF, Nakano M, Abdelfattah AS, Fujiwara M, Ishihara T, Nagai T, et al.: **An expanded palette of genetically encoded Ca(2)(+) indicators**. *Science* 2011, **333**:1888-1891.
27. Heim R, Tsien RY: **Engineering green fluorescent protein for improved brightness, longer wavelengths and fluorescence resonance energy transfer**. *Curr Biol* 1996, **6**:178-182.
28. Zapata-Hommer O, Griesbeck O: **Efficiently folding and circularly permuted variants of the Sapphire mutant of GFP**. *BMC Biotechnol* 2003, **3**:5.
29. Zacharias DA, Violin JD, Newton AC, Tsien RY: **Partitioning of lipid-modified monomeric GFPs into membrane microdomains of live cells**. *Science* 2002, **296**:913-916.
30. Pedelacq JD, Cabantous S, Tran T, Terwilliger TC, Waldo GS: **Engineering and characterization of a superfolder green fluorescent protein**. *Nat Biotechnol* 2006, **24**:79-88.
31. Clavel D, Gotthard G, von Stetten D, De Sanctis D, Pasquier H, Lambert GG, Shaner NC, Royant A: **Structural analysis of the bright monomeric yellow-green fluorescent protein mNeonGreen obtained by directed evolution**. *Acta Crystallogr D Struct Biol* 2016, **72**:1298-1307.
32. Lybarger L, Dempsey D, Patterson GH, Piston DW, Kain SR, Chervenak R: **Dual-color flow cytometric detection of fluorescent proteins using single-laser (488-nm) excitation**. *Cytometry* 1998, **31**:147-152.
33. Barstow B, Ando N, Kim CU, Gruner SM: **Alteration of citrine structure by hydrostatic pressure explains the accompanying spectral shift**. *Proc Natl Acad Sci U S A* 2008, **105**:13362-13366.
34. Rekas A, Alattia JR, Nagai T, Miyawaki A, Ikura M: **Crystal structure of venus, a yellow fluorescent protein with improved maturation and reduced environmental sensitivity**. *J Biol Chem* 2002, **277**:50573-50578.
35. Shaner NC, Lin MZ, McKeown MR, Steinbach PA, Hazelwood KL, Davidson MW, Tsien RY: **Improving the photostability of bright monomeric orange and red fluorescent proteins**. *Nat Methods* 2008, **5**:545-551.
36. Akerboom J, Carreras Calderon N, Tian L, Wabnig S, Prigge M, Tolo J, Gordus A, Orger MB, Severi KE, Macklin JJ, et al.: **Genetically encoded calcium indicators for multi-color neural activity imaging and combination with optogenetics**. *Front Mol Neurosci* 2013, **6**:2.
37. Shemiakina, II, Ermakova GV, Cranfill PJ, Baird MA, Evans RA, Souslova EA, Staroverov DB, Gorokhovatsky AY, Putintseva EV, Gorodnicheva TV, et al.: **A monomeric red fluorescent protein with low cytotoxicity**. *Nat Commun* 2012, **3**:1204.
38. Zhang M, Chang H, Zhang Y, Yu J, Wu L, Ji W, Chen J, Liu B, Lu J, Liu Y, et al.: **Rational design of**

true monomeric and bright photoactivatable fluorescent proteins. *Nat Methods* 2012, **9**:727-729.
39. Yu D, Baird MA, Allen JR, Howe ES, Klassen MP, Reade A, Makhijani K, Song Y, Liu S, Murthy Z, et al.: **A naturally monomeric infrared fluorescent protein for protein labeling in vivo**. *Nat Methods* 2015, **12**:763-765.
40. Tao R, Zhao Y, Chu H, Wang A, Zhu J, Chen X, Zou Y, Shi M, Liu R, Su N, et al.: **Genetically encoded fluorescent sensors reveal dynamic regulation of NADPH metabolism**. *Nat Methods* 2017, **14**:720-728.
41. Fabritius A, Ng D, Kist AM, Erdogan M, Portugues R, Griesbeck O: **Imaging-Based Screening Platform Assists Protein Engineering**. *Cell Chem Biol* 2018, **25**:1554-1561 e1558.
42. Chu J, Haynes RD, Corbel SY, Li P, Gonzalez-Gonzalez E, Burg JS, Ataie NJ, Lam AJ, Cranfill PJ, Baird MA, et al.: **Non-invasive intravital imaging of cellular differentiation with a bright red-excitable fluorescent protein**. *Nat Methods* 2014, **11**:572-578.
43. Hackley CR, Mazzoni EO, Blau J: **cAMPr: A single-wavelength fluorescent sensor for cyclic AMP**. *Sci Signal* 2018, **11**.
44. Wiens MD, Hoffmann F, Chen Y, Campbell RE: **Enhancing fluorescent protein photostability through robot-assisted photobleaching**. *Integr Biol (Camb)* 2018, **10**:419-428.
45. Dean KM, Lubbeck JL, Davis LM, Regmi CK, Chapagain PP, Gerstman BS, Jimenez R, Palmer AE: **Microfluidics-based selection of red-fluorescent proteins with decreased rates of photobleaching**. *Integr Biol (Camb)* 2015, **7**:263-273.
46. Sun F, Zeng J, Jing M, Zhou J, Feng J, Owen SF, Luo Y, Li F, Wang H, Yamaguchi T, et al.: **A Genetically Encoded Fluorescent Sensor Enables Rapid and Specific Detection of Dopamine in Flies, Fish, and Mice**. *Cell* 2018, **174**:481-496 e419.
47. Piatkevich KD, Jung EE, Straub C, Linghu C, Park D, Suk HJ, Hochbaum DR, Goodwin D, Pnevmatikakis E, Pak N, et al.: **A robotic multidimensional directed evolution approach applied to fluorescent voltage reporters**. *Nat Chem Biol* 2018, **14**:352-360.
48. Chavarha M, Villette V, Dimov I, Pradhan L, Evans S, Shi D, Yang R, Chamberland S, Bradley J, Mathieu B, et al.: **Fast two-photon volumetric imaging of an improved voltage indicator reveals electrical activity in deeply located neurons in the awake brain**. *bioRxiv* 2018.
49. Marvin JS, Borghuis BG, Tian L, Cichon J, Harnett MT, Akerboom J, Gordus A, Renninger SL, Chen TW, Bargmann CI, et al.: **An optimized fluorescent probe for visualizing glutamate neurotransmission**. *Nat Methods* 2013, **10**:162-170.
50. Cho JH, Swanson CJ, Chen J, Li A, Lippert LG, Boye SE, Rose K, Sivaramakrishnan S, Chuong CM, Chow RH: **The GCaMP-R Family of Genetically Encoded Ratiometric Calcium Indicators**. *ACS Chem Biol* 2017, **12**:1066-1074.
51. Ast C, Foret J, Oltrogge LM, De Michele R, Kleist TJ, Ho CH, Frommer WB: **Ratiometric Matryoshka biosensors from a nested cassette of green- and orange-emitting fluorescent proteins**. *Nat Commun* 2017, **8**:431.
52. Waters JC: **Accuracy and precision in quantitative fluorescence microscopy**. *J Cell Biol* 2009, **185**:1135-1148.
53. Xu Y, Zou P, Cohen AE: **Voltage imaging with genetically encoded indicators**. *Curr Opin Chem Biol* 2017, **39**:1-10.
54. St-Pierre F, Marshall JD, Yang Y, Gong Y, Schnitzer MJ, Lin MZ: **High-fidelity optical reporting of neuronal electrical activity with an ultrafast fluorescent voltage sensor**. *Nat Neurosci* 2014, **17**:884-889.
55. Perez Koldenkova V, Nagai T: **Genetically encoded Ca(2+) indicators: properties and evaluation**. *Biochim Biophys Acta* 2013, **1833**:1787-1797.
56. Gong Y: **The evolving capabilities of rhodopsin-based genetically encoded voltage indicators**. *Curr Opin Chem Biol* 2015, **27**:84-89.
57. Tian L, Hires SA, Mao T, Huber D, Chiappe ME, Chalasani SH, Petreanu L, Akerboom J, McKinney SA, Schreiter ER, et al.: **Imaging neural activity in worms, flies and mice with improved GCaMP calcium indicators**. *Nat Methods* 2009, **6**:875-881.
58. Oh J, Lee C, Kaang BK: **Imaging and analysis of genetically encoded calcium indicators linking neural circuits and behaviors**. *Korean J Physiol Pharmacol* 2019, **23**:237-249.
59. van der Kant R, Neefjes J: **Small regulators, major consequences - Ca(2)(+) and cholesterol at**

the endosome-ER interface. *J Cell Sci* 2014, **127**:929-938.
60. Pan AC, Borhani DW, Dror RO, Shaw DE: **Molecular determinants of drug-receptor binding kinetics**. *Drug Discov Today* 2013, **18**:667-673.
61. Prinz H: **Hill coefficients, dose-response curves and allosteric mechanisms**. *J Chem Biol* 2010, **3**:37-44.
62. Inoue M, Takeuchi A, Manita S, Horigane SI, Sakamoto M, Kawakami R, Yamaguchi K, Otomo K, Yokoyama H, Kim R, et al.: **Rational Engineering of XCaMPs, a Multicolor GECI Suite for In Vivo Imaging of Complex Brain Circuit Dynamics**. *Cell* 2019, **177**:1346-1360 e1324.
63. Dana H, Sun Y, Mohar B, Hulse BK, Kerlin AM, Hasseman JP, Tsegaye G, Tsang A, Wong A, Patel R, et al.: **High-performance calcium sensors for imaging activity in neuronal populations and microcompartments**. *Nat Methods* 2019.
64. Zhao Y, Hu Q, Cheng F, Su N, Wang A, Zou Y, Hu H, Chen X, Zhou HM, Huang X, et al.: **SoNar, a Highly Responsive NAD+/NADH Sensor, Allows High-Throughput Metabolic Screening of Anti-tumor Agents**. *Cell Metab* 2015, **21**:777-789.
65. Baird GS, Zacharias DA, Tsien RY: **Circular permutation and receptor insertion within green fluorescent proteins**. *Proc Natl Acad Sci U S A* 1999, **96**:11241-11246.
66. Nagai T, Sawano A, Park ES, Miyawaki A: **Circularly permuted green fluorescent proteins engineered to sense Ca2+**. *Proc Natl Acad Sci U S A* 2001, **98**:3197-3202.
67. Sun XR, Badura A, Pacheco DA, Lynch LA, Schneider ER, Taylor MP, Hogue IB, Enquist LW, Murthy M, Wang SS: **Fast GCaMPs for improved tracking of neuronal activity**. *Nat Commun* 2013, **4**:2170.
68. Tallini YN, Ohkura M, Choi BR, Ji G, Imoto K, Doran R, Lee J, Plan P, Wilson J, Xin HB, et al.: **Imaging cellular signals in the heart in vivo: Cardiac expression of the high-signal Ca2+ indicator GCaMP2**. *Proc Natl Acad Sci U S A* 2006, **103**:4753-4758.
69. Shen Y, Dana H, Abdelfattah AS, Patel R, Shea J, Molina RS, Rawal B, Rancic V, Chang YF, Wu L, et al.: **A genetically encoded Ca(2+) indicator based on circularly permutated sea anemone red fluorescent protein eqFP578**. *BMC Biol* 2018, **16**:9.
70. Inoue M, Takeuchi A, Horigane S, Ohkura M, Gengyo-Ando K, Fujii H, Kamijo S, Takemoto-Kimura S, Kano M, Nakai J, et al.: **Rational design of a high-affinity, fast, red calcium indicator R-CaMP2**. *Nat Methods* 2015, **12**:64-70.
71. Ohkura M, Sasaki T, Kobayashi C, Ikegaya Y, Nakai J: **An improved genetically encoded red fluorescent Ca2+ indicator for detecting optically evoked action potentials**. *PLoS One* 2012, **7**:e39933.
72. Berlin S, Carroll EC, Newman ZL, Okada HO, Quinn CM, Kallman B, Rockwell NC, Martin SS, Lagarias JC, Isacoff EY: **Photoactivatable genetically encoded calcium indicators for targeted neuronal imaging**. *Nat Methods* 2015, **12**:852-858.
73. Fosque BF, Sun Y, Dana H, Yang CT, Ohyama T, Tadross MR, Patel R, Zlatic M, Kim DS, Ahrens MB, et al.: **Neural circuits. Labeling of active neural circuits in vivo with designed calcium integrators**. *Science* 2015, **347**:755-760.
74. Moeyaert B, Holt G, Madangopal R, Perez-Alvarez A, Fearey BC, Trojanowski NF, Ledderose J, Zolnik TA, Das A, Patel D, et al.: **Improved methods for marking active neuron populations**. *Nat Commun* 2018, **9**:4440.
75. Wu J, Abdelfattah AS, Miraucourt LS, Kutsarova E, Ruangkittisakul A, Zhou H, Ballanyi K, Wicks G, Drobizhev M, Rebane A, et al.: **A long Stokes shift red fluorescent Ca2+ indicator protein for two-photon and ratiometric imaging**. *Nat Commun* 2014, **5**:5262.
76. Siegel MS, Isacoff EY: **A genetically encoded optical probe of membrane voltage**. *Neuron* 1997, **19**:735-741.
77. Kralj JM, Hochbaum DR, Douglass AD, Cohen AE: **Electrical spiking in Escherichia coli probed with a fluorescent voltage-indicating protein**. *Science* 2011, **333**:345-348.
78. Gautam SG, Perron A, Mutoh H, Knopfel T: **Exploration of fluorescent protein voltage probes based on circularly permuted fluorescent proteins**. *Front Neuroeng* 2009, **2**:14.
79. Barnett L, Platisa J, Popovic M, Pieribone VA, Hughes T: **A fluorescent, genetically-encoded voltage probe capable of resolving action potentials**. *PLoS One* 2012, **7**:e43454.
80. Abdelfattah AS, Farhi SL, Zhao Y, Brinks D, Zou P, Ruangkittisakul A, Platisa J, Pieribone VA, Ballanyi K, Cohen AE, et al.: **A Bright and Fast Red Fluorescent Protein Voltage Indicator**

That Reports Neuronal Activity in Organotypic Brain Slices. *J Neurosci* 2016, **36**:2458-2472.

81. St-Pierre F, Chavarha M, Lin MZ: **Designs and sensing mechanisms of genetically encoded fluorescent voltage indicators**. *Curr Opin Chem Biol* 2015, **27**:31-38.
82. Marvin JS, Scholl B, Wilson DE, Podgorski K, Kazemipour A, Muller JA, Schoch S, Quiroz FJU, Rebola N, Bao H, et al.: **Stability, affinity, and chromatic variants of the glutamate sensor iGluSnFR**. *Nat Methods* 2018, **15**:936-939.
83. Helassa N, Durst CD, Coates C, Kerruth S, Arif U, Schulze C, Wiegert JS, Geeves M, Oertner TG, Torok K: **Ultrafast glutamate sensors resolve high-frequency release at Schaffer collateral synapses**. *Proc Natl Acad Sci U S A* 2018, **115**:5594-5599.
84. Shivange AV, Borden PM, Muthusamy AK, Nichols AL, Bera K, Bao H, Bishara I, Jeon J, Mulcahy MJ, Cohen B, et al.: **Determining the pharmacokinetics of nicotinic drugs in the endoplasmic reticulum using biosensors**. *J Gen Physiol* 2019.
85. Marvin JS, Shimoda Y, Magloire V, Leite M, Kawashima T, Jensen TP, Kolb I, Knott EL, Novak O, Podgorski K, et al.: **A genetically encoded fluorescent sensor for in vivo imaging of GABA**. *Nat Methods* 2019.
86. Tanaka M, Sun F, Li Y, Mooney R: **A mesocortical dopamine circuit enables the cultural transmission of vocal behaviour**. *Nature* 2018, **563**:117-120.
87. Jing M, Zhang P, Wang G, Feng J, Mesik L, Zeng J, Jiang H, Wang S, Looby JC, Guagliardo NA, et al.: **A genetically encoded fluorescent acetylcholine indicator for in vitro and in vivo studies**. *Nat Biotechnol* 2018, **36**:726-737.
88. Feng J, Zhang C, Lischinsky JE, Jing M, Zhou J, Wang H, Zhang Y, Dong A, Wu Z, Wu H, et al.: **A Genetically Encoded Fluorescent Sensor for Rapid and Specific In Vivo Detection of Norepinephrine**. *Neuron* 2019.
89. Patriarchi T, Cho JR, Merten K, Howe MW, Marley A, Xiong WH, Folk RW, Broussard GJ, Liang R, Jang MJ, et al.: **Ultrafast neuronal imaging of dopamine dynamics with designed genetically encoded sensors**. *Science* 2018, **360**.
90. Gutscher M, Pauleau AL, Marty L, Brach T, Wabnitz GH, Samstag Y, Meyer AJ, Dick TP: **Real-time imaging of the intracellular glutathione redox potential**. *Nat Methods* 2008, **5**:553-559.
91. Fan Y, Makar M, Wang MX, Ai HW: **Monitoring thioredoxin redox with a genetically encoded red fluorescent biosensor**. *Nat Chem Biol* 2017, **13**:1045-1052.
92. Hung YP, Albeck JG, Tantama M, Yellen G: **Imaging cytosolic NADH-NAD(+) redox state with a genetically encoded fluorescent biosensor**. *Cell Metab* 2011, **14**:545-554.
93. Zhao Y, Jin J, Hu Q, Zhou HM, Yi J, Yu Z, Xu L, Wang X, Yang Y, Loscalzo J: **Genetically encoded fluorescent sensors for intracellular NADH detection**. *Cell Metab* 2011, **14**:555-566.
94. Cambronne XA, Stewart ML, Kim D, Jones-Brunette AM, Morgan RK, Farrens DL, Cohen MS, Goodman RH: **Biosensor reveals multiple sources for mitochondrial NAD(+)**. *Science* 2016, **352**:1474-1477.
95. Wang W, Fang H, Groom L, Cheng A, Zhang W, Liu J, Wang X, Li K, Han P, Zheng M, et al.: **Superoxide flashes in single mitochondria**. *Cell* 2008, **134**:279-290.
96. Zhao BS, Liang Y, Song Y, Zheng C, Hao Z, Chen PR: **A highly selective fluorescent probe for visualization of organic hydroperoxides in living cells**. *J Am Chem Soc* 2010, **132**:17065-17067.
97. Belousov VV, Fradkov AF, Lukyanov KA, Staroverov DB, Shakhbazov KS, Terskikh AV, Lukyanov S: **Genetically encoded fluorescent indicator for intracellular hydrogen peroxide**. *Nat Methods* 2006, **3**:281-286.
98. Markvicheva KN, Bilan DS, Mishina NM, Gorokhovatsky AY, Vinokurov LM, Lukyanov S, Belousov VV: **A genetically encoded sensor for H2O2 with expanded dynamic range**. *Bioorg Med Chem* 2011, **19**:1079-1084.
99. Bilan DS, Pase L, Joosen L, Gorokhovatsky AY, Ermakova YG, Gadella TW, Grabher C, Schultz C, Lukyanov S, Belousov VV: **HyPer-3: a genetically encoded H(2)O(2) probe with improved performance for ratiometric and fluorescence lifetime imaging**. *ACS Chem Biol* 2013, **8**:535-542.
100. Ermakova YG, Bilan DS, Matlashov ME, Mishina NM, Markvicheva KN, Subach OM, Subach FV, Bogeski I, Hoth M, Enikolopov G, et al.: **Red fluorescent genetically encoded indicator for**

intracellular hydrogen peroxide. *Nat Commun* 2014, **5**:5222.
101. Tarrago L, Peterfi Z, Lee BC, Michel T, Gladyshev VN: **Monitoring methionine sulfoxide with stereospecific mechanism-based fluorescent sensors**. *Nat Chem Biol* 2015, **11**:332-338.
102. Ostergaard H, Henriksen A, Hansen FG, Winther JR: **Shedding light on disulfide bond formation: engineering a redox switch in green fluorescent protein**. *EMBO J* 2001, **20**:5853-5862.
103. Hanson GT, Aggeler R, Oglesbee D, Cannon M, Capaldi RA, Tsien RY, Remington SJ: **Investigating mitochondrial redox potential with redox-sensitive green fluorescent protein indicators**. *J Biol Chem* 2004, **279**:13044-13053.
104. Shokhina AG, Kostyuk AI, Ermakova YG, Panova AS, Staroverov DB, Egorov ES, Baranov MS, van Belle GJ, Katschinski DM, Belousov VV, et al.: **Red fluorescent redox-sensitive biosensor Grx1-roCherry**. *Redox Biol* 2019, **21**:101071.
105. Piattoni CV, Sardi F, Klein F, Pantano S, Bollati-Fogolin M, Comini M: **New red-shifted fluorescent biosensor for monitoring intracellular redox changes**. *Free Radic Biol Med* 2019, **134**:545-554.
106. Fan Y, Chen Z, Ai HW: **Monitoring redox dynamics in living cells with a redox-sensitive red fluorescent protein**. *Anal Chem* 2015, **87**:2802-2810.
107. Tewson PH, Martinka S, Shaner NC, Hughes TE, Quinn AM: **New DAG and cAMP Sensors Optimized for Live-Cell Assays in Automated Laboratories**. *J Biomol Screen* 2016, **21**:298-305.
108. Harada K, Ito M, Wang X, Tanaka M, Wongso D, Konno A, Hirai H, Hirase H, Tsuboi T, Kitaguchi T: **Red fluorescent protein-based cAMP indicator applicable to optogenetics and in vivo imaging**. *Sci Rep* 2017, **7**:7351.
109. Ohta Y, Furuta T, Nagai T, Horikawa K: **Red fluorescent cAMP indicator with increased affinity and expanded dynamic range**. *Sci Rep* 2018, **8**:1866.
110. Nausch LW, Ledoux J, Bonev AD, Nelson MT, Dostmann WR: **Differential patterning of cGMP in vascular smooth muscle cells revealed by single GFP-linked biosensors**. *Proc Natl Acad Sci U S A* 2008, **105**:365-370.
111. Tewson P, Westenberg M, Zhao Y, Campbell RE, Quinn AM, Hughes TE: **Simultaneous detection of Ca2+ and diacylglycerol signaling in living cells**. *PLoS One* 2012, **7**:e42791.
112. Tewson PH, Quinn AM, Hughes TE: **A multiplexed fluorescent assay for independent second-messenger systems: decoding GPCR activation in living cells**. *J Biomol Screen* 2013, **18**:797-806.
113. Sakaguchi R, Endoh T, Yamamoto S, Tainaka K, Sugimoto K, Fujieda N, Kiyonaka S, Mori Y, Morii T: **A single circularly permuted GFP sensor for inositol-1,3,4,5-tetrakisphosphate based on a split PH domain**. *Bioorg Med Chem* 2009, **17**:7381-7386.
114. Berg J, Hung YP, Yellen G: **A genetically encoded fluorescent reporter of ATP:ADP ratio**. *Nat Methods* 2009, **6**:161-166.
115. Tantama M, Martinez-Francois JR, Mongeon R, Yellen G: **Imaging energy status in live cells with a fluorescent biosensor of the intracellular ATP-to-ADP ratio**. *Nat Commun* 2013, **4**:2550.
116. Yaginuma H, Kawai S, Tabata KV, Tomiyama K, Kakizuka A, Komatsuzaki T, Noji H, Imamura H: **Diversity in ATP concentrations in a single bacterial cell population revealed by quantitative single-cell imaging**. *Sci Rep* 2014, **4**:6522.
117. Lobas MA, Tao R, Nagai J, Kronschlager MT, Borden PM, Marvin JS, Looger LL, Khakh BS: **A genetically encoded single-wavelength sensor for imaging cytosolic and cell surface ATP**. *Nat Commun* 2019, **10**:711.
118. Bianchi-Smiraglia A, Rana MS, Foley CE, Paul LM, Lipchick BC, Moparthy S, Moparthy K, Fink EE, Bagati A, Hurley E, et al.: **Internally ratiometric fluorescent sensors for evaluation of intracellular GTP levels and distribution**. *Nat Methods* 2017, **14**:1003-1009.
119. Zhang C, Ye BC: **A single fluorescent protein-based sensor for in vivo 2-oxogluatarate detection in cell**. *Biosens Bioelectron* 2014, **54**:15-19.
120. Honda Y, Kirimura K: **Generation of circularly permuted fluorescent-protein-based indicators for in vitro and in vivo detection of citrate**. *PLoS One* 2013, **8**:e64597.
121. Hu H, Gu Y, Xu L, Zou Y, Wang A, Tao R, Chen X, Zhao Y, Yang Y: **A genetically encoded toolkit for**

tracking live-cell histidine dynamics in space and time. *Sci Rep* 2017, **7**:43479.
122. Hu H, Wei Y, Wang D, Su N, Chen X, Zhao Y, Liu G, Yang Y: **Glucose monitoring in living cells with single fluorescent protein-based sensors**. *RSC Advances* 2018, **8**:2485-2489.
123. Keller JP, Marvin JS, Lacin H, Lemon WC, Shea J, Kim S, Lee RT, Koyama M, Keller PJ, Looger LL: **In vivo glucose imaging in multiple model organisms with an engineered single-wavelength sensor**. *bioRxiv* 2019.
124. Alicea I, Marvin JS, Miklos AE, Ellington AD, Looger LL, Schreiter ER: **Structure of the Escherichia coli phosphonate binding protein PhnD and rationally optimized phosphonate biosensors**. *J Mol Biol* 2011, **414**:356-369.
125. Qin Y, Sammond DW, Braselmann E, Carpenter MC, Palmer AE: **Development of an Optical Zn(2+) Probe Based on a Single Fluorescent Protein**. *ACS Chem Biol* 2016, **11**:2744-2751.
126. Fudge DH, Black R, Son L, LeJeune K, Qin Y: **Optical Recording of Zn(2+) Dynamics in the Mitochondrial Matrix and Intermembrane Space with the GZnP2 Sensor**. *ACS Chem Biol* 2018, **13**:1897-1905.
127. Kawai Y, Sato M, Umezawa Y: **Single color fluorescent indicators of protein phosphorylation for multicolor imaging of intracellular signal flow dynamics**. *Anal Chem* 2004, **76**:6144-6149.
128. Mao YT, Zhu JX, Hanamura K, Iurilli G, Datta SR, Dalva MB: **Filopodia Conduct Target Selection in Cortical Neurons Using Differences in Signal Kinetics of a Single Kinase**. *Neuron* 2018, **98**:767-782 e768.
129. De Michele R, Ast C, Loque D, Ho CH, Andrade S, Lanquar V, Grossmann G, Gehne S, Kumke MU, Frommer WB: **Fluorescent sensors reporting the activity of ammonium transceptors in live cells**. *Elife* 2013, **2**:e00800.
130. Ast C, De Michele R, Kumke MU, Frommer WB: **Single-fluorophore membrane transport activity sensors with dual-emission read-out**. *Elife* 2015, **4**:e07113.
131. Ashraf KU, Josts I, Mosbahi K, Kelly SM, Byron O, Smith BO, Walker D: **The Potassium Binding Protein Kbp Is a Cytoplasmic Potassium Sensor**. *Structure* 2016, **24**:741-749.
132. Miyawaki A, Niino Y: **Molecular spies for bioimaging--fluorescent protein-based probes**. *Mol Cell* 2015, **58**:632-643.
133. Li T, Chen ZJ: **The cGAS-cGAMP-STING pathway connects DNA damage to inflammation, senescence, and cancer**. *J Exp Med* 2018, **215**:1287-1299.
134. Hertel F, Mo GC, Duwe S, Dedecker P, Zhang J: **RefSOFI for Mapping Nanoscale Organization of Protein-Protein Interactions in Living Cells**. *Cell Rep* 2016, **14**:390-400.
135. Guo Y, Li D, Zhang S, Yang Y, Liu JJ, Wang X, Liu C, Milkie DE, Moore RP, Tulu US, et al.: **Visualizing Intracellular Organelle and Cytoskeletal Interactions at Nanoscale Resolution on Millisecond Timescales**. *Cell* 2018, **175**:1430-1442 e1417.
136. Huang X, Fan J, Li L, Liu H, Wu R, Wu Y, Wei L, Mao H, Lal A, Xi P, et al.: **Fast, long-term, super-resolution imaging with Hessian structured illumination microscopy**. *Nat Biotechnol* 2018, **36**:451-459.